sustainability

MDPI

Article

Energy and Environmental Analyses of a Solar–Gas Turbine Combined Cycle with Inlet Air Cooling

Ahmad M. Abubaker [1,*], Adnan Darwish Ahmad [1], Binit B. Singh [2], Yaman M. Manaserh [3], Loiy Al-Ghussain [4,*], Nelson K. Akafuah [1] and Kozo Saito [1]

[1] Institute of Research for Technology Development (IR4TD), University of Kentucky, Lexington, KY 40506, USA; adnandarwish@uky.edu (A.D.A.); nelson.akafuah@uky.edu (N.K.A.); ksaito@uky.edu (K.S.)
[2] Department of Mechanical Engineering, University of Minnesota Twin Cities, Minneapolis, MN 55414, USA; sing0815@umn.edu
[3] Department of Mechanical Engineering, ES2 Center, Binghamton University-SUNY, Binghamton, NY 13902, USA; yyaseen1@binghamton.edu
[4] Energy Systems and Infrastructure Analysis Division, Argonne National Laboratory, Lemont, IL 60439, USA
* Correspondence: ahmadmahmud19@hotmail.com (A.M.A.); lalghussain@anl.gov (L.A.-G.)

Abstract: Sensitivity to ambient air temperatures, consuming a large amount of fuel, and wasting a significant amount of heat dumped into the ambient atmosphere are three major challenges facing gas turbine power plants. This study was conducted to simultaneously solve all three aforementioned GT problems using solar energy and introducing a new configuration that consists of solar preheating and inlet-air-cooling systems. In this study, air was preheated at a combustion chamber inlet using parabolic trough collectors. Then, inlet air to the compressor was cooled by these collectors by operating an absorption cooling cycle. At the design point conditions, this novel proposed integration resulted in a 6.87% relative increase in generated power and a 10.53% relative decrement in fuel consumption, achieving a 19.45% relative increment in the plant's thermal efficiency. This was accompanied by a reduction of 0.026 kg/s, 4.2 kg/s, and 0.278 kg/s in CO_2, CO, and NOx emissions, respectively. Finally, spider diagrams were employed to assess the impact of the operating parameters on the overall system's performance and its associated environmental implications.

Keywords: combined-cycle power plants; solar power; parabolic trough collector; absorption cooling unit; decarbonization

check for updates

Citation: Abubaker, A.M.; Ahmad, A.D.; Singh, B.B.; Manaserh, Y.M.; Al-Ghussain, L.; Akafuah, N.K.; Saito, K. Energy and Environmental Analyses of a Solar–Gas Turbine Combined Cycle with Inlet Air Cooling. *Sustainability* **2024**, *16*, 6229. https://doi.org/10.3390/su16146229

Academic Editor: Firoz Alam

Received: 12 June 2024
Revised: 9 July 2024
Accepted: 18 July 2024
Published: 21 July 2024

Copyright: © 2024 by the authors. Licensee MDPI, Basel, Switzerland. This article is an open access article distributed under the terms and conditions of the Creative Commons Attribution (CC BY) license (https://creativecommons.org/licenses/by/4.0/).

1. Introduction

Solar power has promising potential, but it faces a few challenges, including high intermittency [1] and low efficiency in direct electrical generation using concentrated solar power in PTCs due to the limitations of the maximum allowable temperature in the solar field troughs. The organic Rankine cycle driven by solar collectors, for example, suffers from less than 10% efficiency [2]. Hybridization with fossil fuel systems is recommended to enhance solar energy stability and minimize fuel consumption [3]. Gas turbines operated by NG, a good candidate for hybridization [4], suffer from three major problems: the significant amount of waste heat released into the ambient atmosphere, the excessive amount of fuel required, and sensitivity to ambient air temperature. The following explains each of these three problems.

1.1. The First Problem of GTs: Waste Heat

The exhaust temperature of a gas turbine operating on natural gas could range from 350 °C to 650 °C [5]. Utilization of the waste heat could enhance the thermal efficiency of gas turbines [6]. Adopting cogeneration systems by combining the GT cycle coupled with a secondary cycle is extremely favorable, due to the high temperatures of exhaust gases

from a GT, which exceed 500 °C [7]. Dabwan et al. [8] proposed using waste heat to cool the compressor's inlet air utilizing absorption chillers, increasing power output by 19% and overall system efficiency by 2.3%.

1.2. The Second Problem of GTs: Excessive Amount of Fuel

Gas turbines are responsible for a considerable portion of NG consumption growth worldwide; in 2019, global NG consumption growth was approximately 2.1% [9]. The use of NG for power generation has been consistently increasing in the USA. There was a 7% rise in the consumption of NG for power generation in the USA from 2022 to 2023 [10]. In addition, gas turbine power plants use a large amount of air while operating, with one extreme case report using up to 290 kg/s of air in the combustion chamber [11], in which the temperature of combustion gases can be higher than 1800 °C, releasing an enormous amount of environmentally harmful gases such as CO_2, CO, and NOx [12]. The implementation of carbon mitigation policies such as cap-and-trade systems is being incrementally noticed worldwide. Gas turbines, for instance, pour extensive amounts of carbon monoxide and dioxide into the atmosphere. Therefore, research is suggesting new strategies to cut down the pollution caused by power generation systems. For instance, Dimitriadis et al. [13] proposed a bi-level optimization framework to enhance and optimize order strategies for gas-fired power plants based on weighting the market of electricity and natural fuel. An emission trading system (ETS) would be also a good candidate market-based tool to create motivation to mitigate greenhouse gas emissions and save natural gas reserves.

In the case of a sole GT power plant, waste heat can be used to preheat inlet air using a recuperator, improving the GT cycle's thermal efficiency. Another way of improving the efficiency of GT power plants is to use solar energy. For instance, Al-Otoom et al. [14] used PTC to increase the temperature of the air entering the CC, decreasing NG consumption by 64%.

1.3. The Third Problem of GTs: Sensitivity to Ambient Air Temperature

1.3.1. Ambient Air Temperature Control by Inlet-Air-Cooling Techniques

An increase in the ambient temperature causes a drop in GT output power [15] since power output heavily depends on the air mass flow rate, creating the third problem. The specific volume of air at the air compressor's inlet increases by the increase in ambient temperature, requiring more power to be compressed. Extremely hot climate regions whose daily high temperature can reach 50 °C often use gas turbine power plants. For instance, it was reported that a 0.74% and 0.1% decrease in GT power output and overall thermal efficiency, respectively, are expected if the ambient temperature increases by 1 °C [16]. In hot-weather regions, the electricity demand is typically accompanied with an increment in ambient temperature due to air conditioning load [17], suggesting IAC could be a solution, either by evaporation to reduce temperature and increase humidity or refrigeration to only reduce temperature.

Many gas turbines are combined with HRUs that drive steam turbine STs to use the most power from waste heat, making the ACU limited and unable to reach the ideal inlet air temperature of 5 °C [18] because the condensation of sulfuric acid [19], corrosive to the pipes of the heat exchangers [20], will occur below this ideal temperature. Darwish Ahmad et al. [7] managed to utilize this small amount of waste heat in the GTCC and successfully overcame these two problems by proposing a hybrid IAC system that uses ACU and MCU. The absorption chilling unit, limited by low waste heat, can reduce the ambient temperature to a certain degree, after which the MCU can extend the temperature drop until it reaches 5 °C.

1.3.2. The Effect of Inlet Air Cooling on Fuel Consumption

IAC is efficient in boosting power-plant-generated power and improving its efficiency. On the other hand, cooling the air that enters the compressor decreases the temperature of

air leaving the compressor, considering its polytropic efficiency [21], and, hence, cooler air enters the CC. Consequently, the amount of energy that needs to be introduced to maintain a constant turbine inlet temperature at the design point will increase [22]. This means that higher amounts of fuel will be introduced in the CC, hence leading to higher amounts of pollutant emissions. Najjar and Al-Zoghool [23] showed that the annual fuel cost would increase by USD 191 K and USD 184 K when employing mechanical and absorption cooling systems, respectively.

1.4. Problem Statement and Motivation for This Study

Previous studies focused on one or two of these challenges simultaneously, but none of these studies addressed these challenges at the same time. For instance, cooling the air entering a compressor to boost generated power has extensively been investigated. Even though it introduces reasonable control over the air temperature at the compressor's inlet, the amount of fuel used in the CC considerably increases [24]. In addition, researchers have investigated utilizing waste heat to preheat the CC's inlet air and operating IAC cycles, which are thermally driven to improve power plant efficiency [25]. In some cases, researchers even investigated integrating renewable resources into existing power plants [26]. This proposed work will consider not only the importance of research from the position of applying a gas turbine whose intake system is the subject of utilization but also the utilization of fuel consumption by increasing air temperature before the combustion chamber. However, and most importantly, as explained by Cho and Saito [27], these three problems are nonlinear—the same as TPS. Therefore, they should be investigated simultaneously and addressed together. Hence, this study aims to investigate these issues simultaneously by considering the following:

- An actual GTCC was integrated with a PTC. Hence, the initial GT dilemma was resolved using a steam generator with a heat recovery system to operate an ST to generate extra power.
- A new CSS was introduced with two SHEs powered by PTCs to address the second and third dilemmas.
    - The first solar heat exchanger, SHE1, was utilized to preheat the air that enters the combustion chamber to decrease the amount of fuel the system uses, hence further decarbonizing the system.
    - The second solar heat exchanger, SHE2, operated an ACU to decrease the compressor's inlet air temperature to 5 °C. According to the recommendation, the air temperature cooling was limited to this temperature to attain the highest output power while eliminating the possibility of ice formation on the compressor's blades.

Researchers [28,29] have used existing power plant performance to validate their theoretical configurations and predictions. Following this methodology, the Al-Qatrana GTCC located in Jordan was adopted as an actual case study to be examined in this paper to confirm the prediction and reliability of the developed code. The current Al-Qatrana power plant is highly affected by high ambient temperatures and large fuel consumption rates [30]. The proposed system offers an environmentally friendly and sustainable resolution to solve the problem associated with increased fuel consumption caused by the IAC, which has not been addressed before.

The novelty and major contributions of this study can be summarized as follows:

- A solution that simultaneously addresses the three problems of GTCC plants using solar energy is presented.
- The energy of the integration is explored by employing thermodynamic, heat transfer equations, and semi-empirical equations.
- The environmental aspects of the combined cycle are improved by reducing greenhouse gas emissions and pollutants (CO, CO_2, and NOx).

- A parametric spider diagram study of the major operating parameters is used to examine their impact on the power plant's performance and pollutant emissions.

Figure 1 summarizes the methodology adopted in this study.

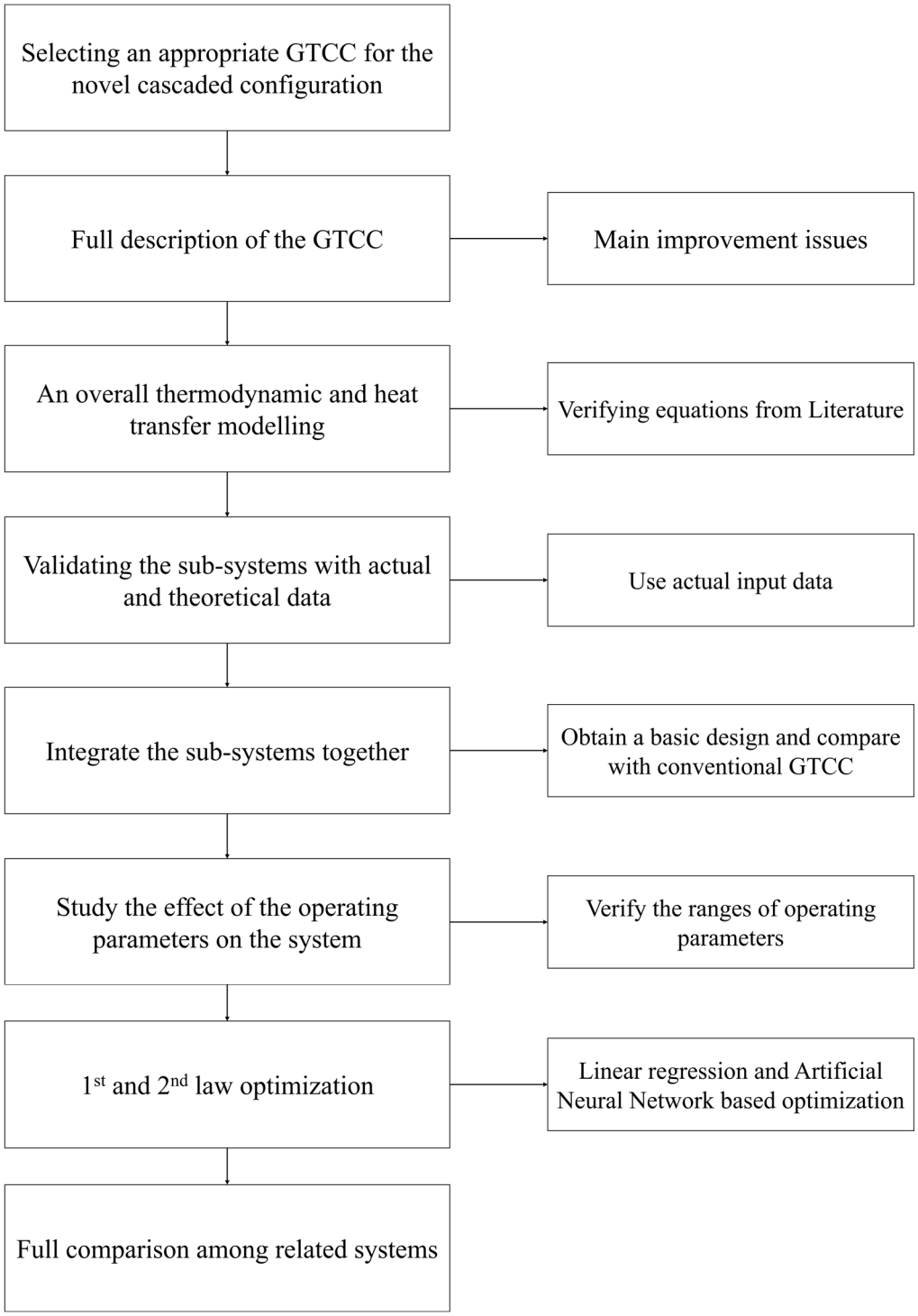

Figure 1. Flow diagram of the research structure procedure.

The following sections will provide a detailed description of the proposed system (Section 2), an explanation of the modeling methods used for all system components, and details of the performance analysis conducted.

2. System Description

As mentioned, Al-Qatrana was selected as an actual GTCC, since its operational conditions can vary within an acceptable range, to find the best operating conditions for integration with the CSS [28]. Further information about the power plant can be found in [31]. Waste heat from GTs is utilized in one double-pressure level HRSG connected to high- and low-pressure STs to produce power. Figure 2 shows the proposed integrated GTCC combined with the PTC system and ACU system (PACC). Two solar heat exchangers are cascaded to preheat the compressed air before entering the CC and operating the absorption chiller.

The proposed system consists of a gas turbine, where, after the compressor, there is a solar parabolic collector station that increases the temperature further before entering the combustion chamber. This can reduce the fuel used while keeping the operational temperature at the design point. The remaining heat from the parabolic solar collectors was utilized in an absorption cooling unit to reduce the ambient temperature before entering the compressor to reduce its power consumption. In Heller et al. [32], the first original solar-powered gas turbine system was installed and tested in the CESA-1 tower facility at Plataforma Solar de Almeri'a (PSA) in Spain.

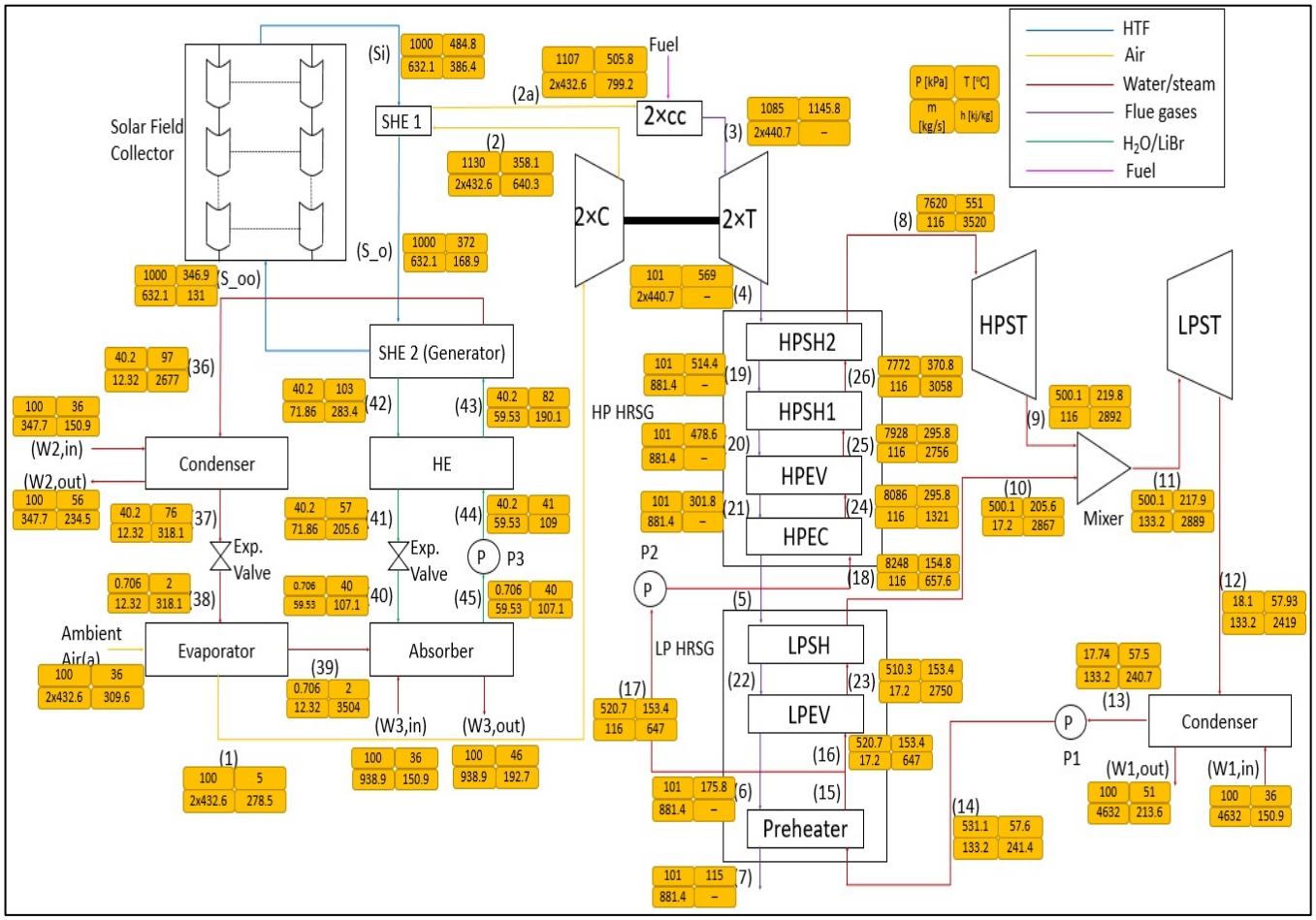

Figure 2. Schematic diagram of the main system [33].

To ensure the system's reliability, PACC was divided into four subsystems, GT, HRU, PTC, and ACU, and each subsystem was validated with the literature data. Finally, the overall PACC integration of all subsystems was validated using EES software 9.4.7.8 [34].

Readers are referred to Figure 2, which follows the sequence of the PACC. The GT sequence is summarized in Figure 3. After air is pressurized in the compressor, it is heated up in stages by concentrated solar panels and then by the combustion chamber via combustion with fuel. High-energy combusted gases are utilized in the turbine. Since the fuel input is decreased due to the preheating in SHE2, the mass flow rate of flue gas decreases proportionally, and power generation in the STs is expected to reduce. The subsequent HRSG starting from pump1 is illustrated in Figure 4. As for the CSP system, PTCs are used to reflect the solar radiation incident on a PTC absorber in which the HTF (molten salt) flows. The sequence of the CSP system is illustrated in Figure 5. As for the ACU, a single-effect LiBr/H_2O is considered instead of ammonia/water for poisonousness conundrums. Also, vapor water is considered a refrigerant. Finally, the remaining sequence of the PACC is shown in Figure 6. These diagrams can be interpreted by the main system schematic diagram in Figure 2.

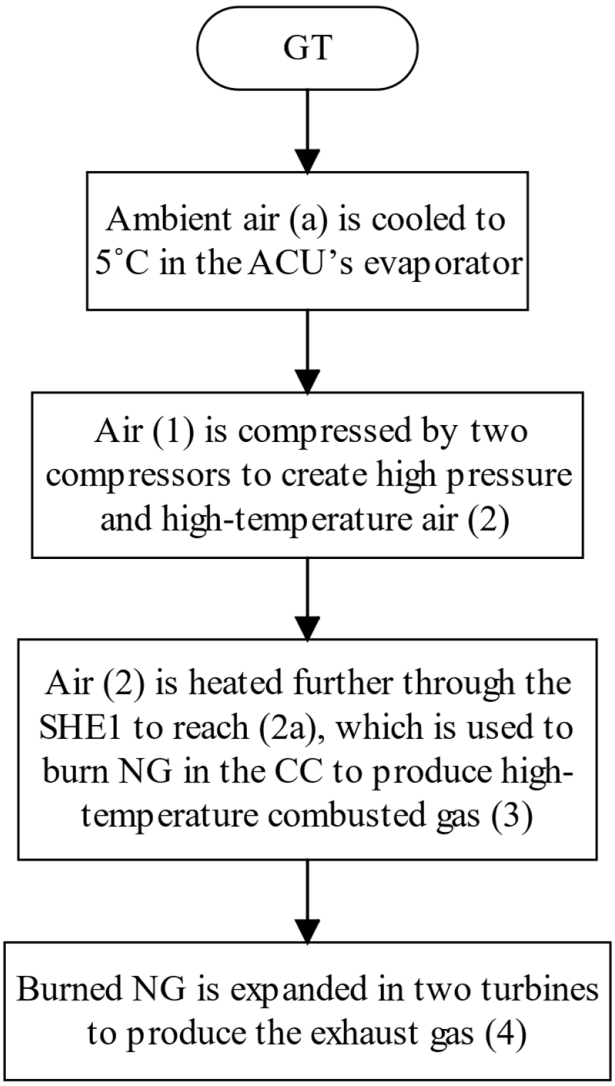

Figure 3. Description of GT sequence.

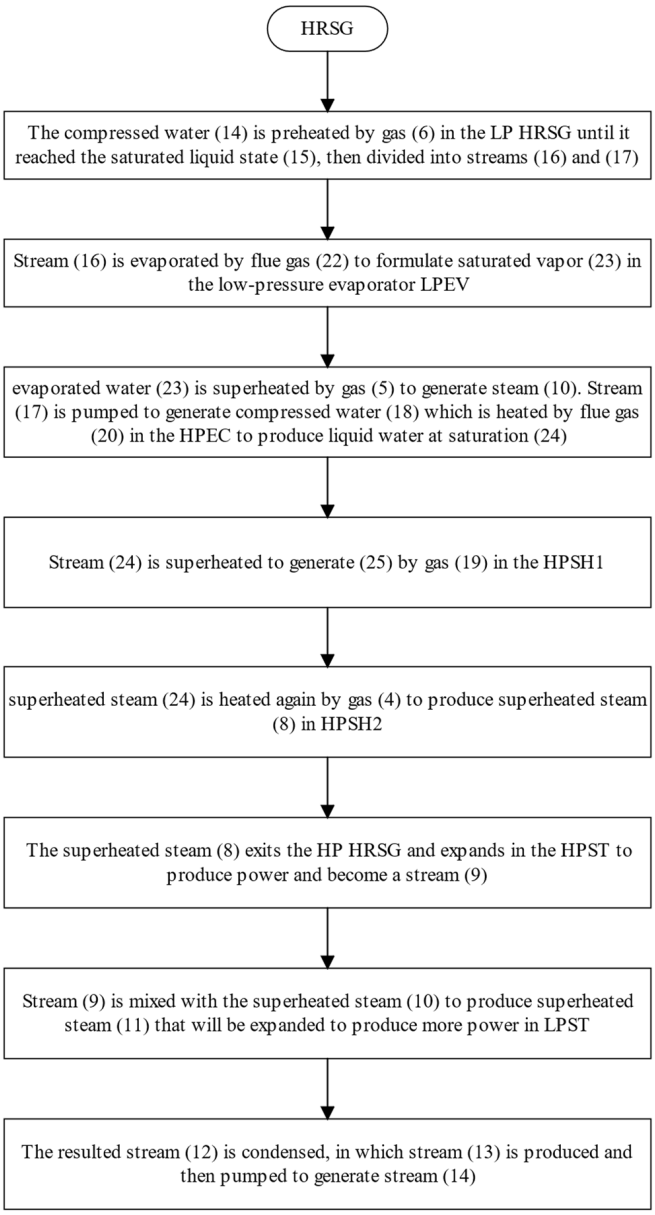

Figure 4. HRSG sequence description.

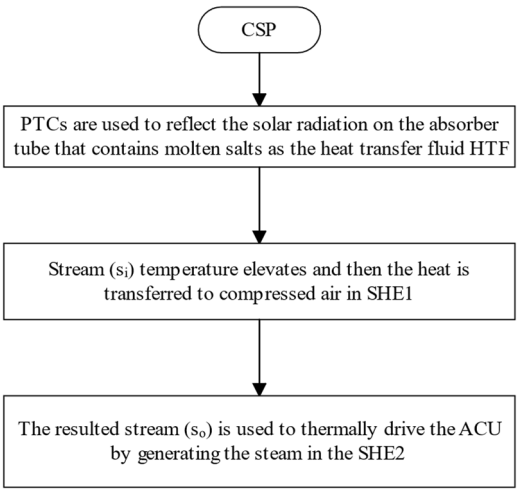

Figure 5. Description of CSP sequence.

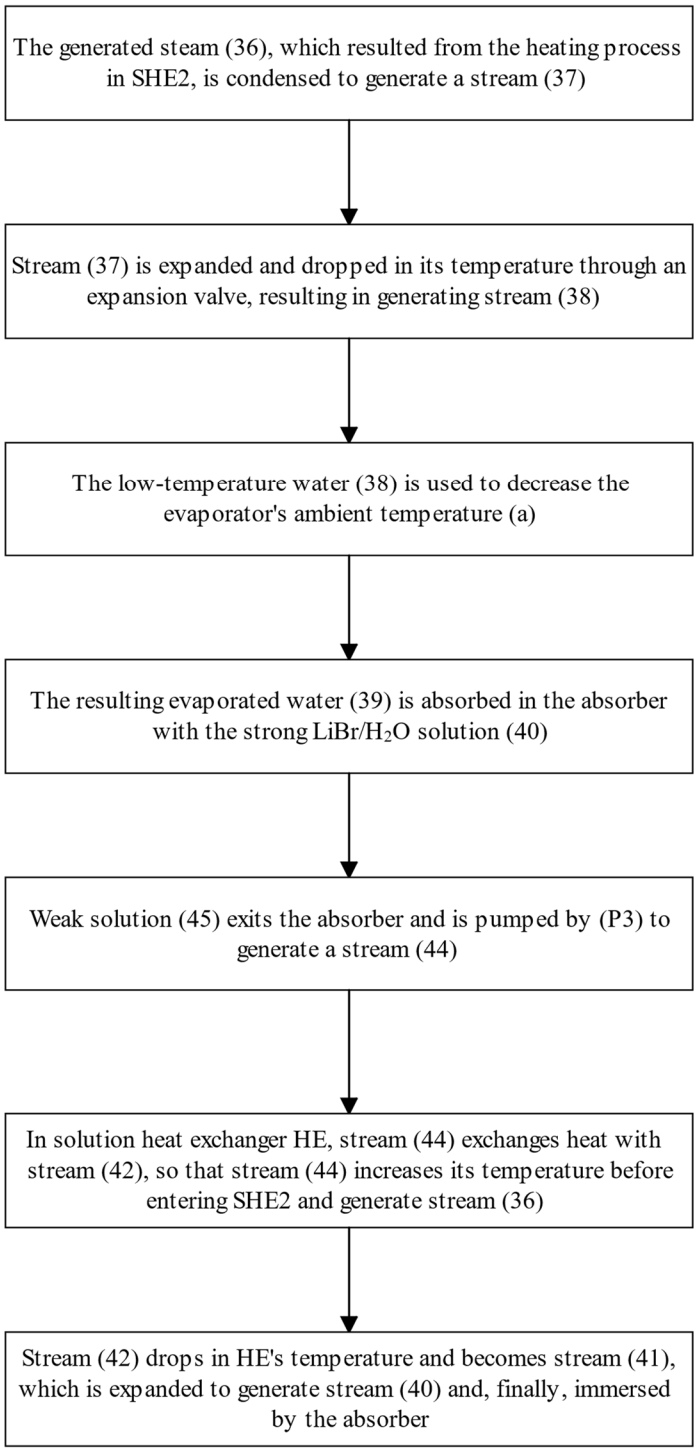

Figure 6. Description of the remaining sequence in the PACC.

3. Power Plant Modeling

The modeling and performance evaluation of the GTCC, PTC, ACU, and cascaded solar heat exchangers are discussed in this section. The assumption, operating, and ambient conditions at the design point for the Al-Qatrana plant are summarized in Table 1. The assumptions made for the subsystems are adopted from [35] GTCC, ref. [36], PTC, and ACU [7], while the integration of all three components is our original work and is shown here for the first time.

Table 1. Assumption, operating, and ambient conditions at the design point.

Ambient Conditions [30]	
Ambient air temperature	36 °C
Ambient air pressure	100 kPa
GT [7]	
Model	SGT6-2000E
Number of gas turbines	2
Pressure ratio	11.3
CC efficiency, η_{CC}	98%
Natural gas LHV	49,322 kJ/s
GT exhaust temperature, T_4	569 °C
Air mass flowrate for each GT, m_a	432.6 kg/s
HRSG [7]	
Isentropic efficiency of STs	85%
Efficiency of pumps	80%
Evaporation pressure in HP HRSG	8248 kPa
Evaporation pressure in LP HRSG	531.1 kPa
Steam flowrate in HP HRSG, m_8	116 kg/s
Steam flowrate in LP HRSG, m_{10}	17.2 kg/s
Pressure ratio in HP HRSG, $r_{p,HP}$	15.8
Pressure ratio LP HRSG, r_{pLP}	30
Pressure drop in heat exchanger	2%

Figure 7 shows a flow chart for the interaction among the units and how each system can contribute to the other. The gas turbine starts to operate the HRU, which results in enhancing the overall performance by recovering heat from exhaust gases and generating additional power using STs. Then, PTC drives the ACU through SHE2 to boost the GT-generated power by reducing the compressor's power consumption. Finally, SHE1 heats the air before flowing into the CC to decrease the fuel consumption.

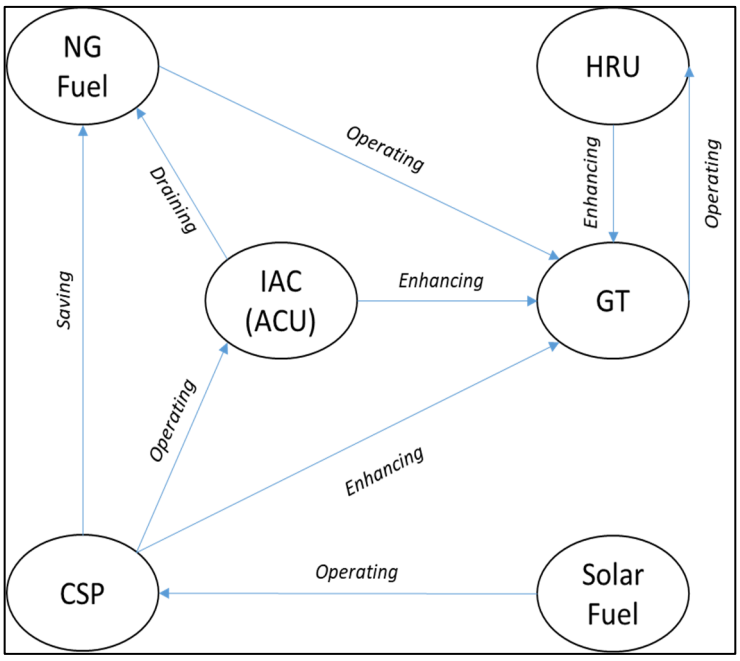

Figure 7. Flowchart for the proposed system.

Here, we built our mathematical model for the cycle to analyze the performance of the proposed system thermodynamically. Assumptions for each unit of the PACC were made while conducting this study as follows:

- All PACC components are adiabatic.
- Steady-state conditions are achieved.
- Negligible kinetic and potential energies are achieved [37], since the cooling load that is required by the ACU and the heat input required for the compressed air are acquired from the GTs.
- A pressure drop was assumed to occur through each heat exchanger unit [24].

3.1. Modeling of GT Unit

Gas turbines have the highest energy production in the PACC; however, the power generation rate can be further improved at high ambient temperatures. The governing equations to model GT components, compressors, CCs, and turbines for two GTs were adopted from [38], and GTs are shown in Appendix A to simulate the GT operation numerically.

3.2. Modeling of the HRSG Unit

The input energy for the HRSG unit comes directly from the GT waste heat and the PACC, which affects the total mass flow, whose small part comes from the fuel in the total energy output in the STs. While modeling the HRSG, a pressure drop was assumed to occur through each heat exchanger unit [24]. The equations used for calculating the properties of the different states across the heat exchanger are given in Appendix A.

3.3. Modeling of the CSP Unit

Concentrated solar power (CSP) consists of parabolic trough collectors that work in a trace mode, Col_r collector modules in parallel, and Col_s series, whose parameters substantially affect the active solar collecting area. The amount of HTF that passes through each Col_r is fixed; hence, using larger Col_r number results in a higher HTF mass flowrate, while increasing the Col_s results in increasing the HTF output temperature [39]. Luz 3rd generation parabolic trough collector, LS-3, was selected based on the recommendation by [40] with the specifications reported in [41].

Solar radiation fluctuates throughout the day and varies from one place to another. Some models use the highest potential [42], while using the annual average seems reasonable. Therefore, we obtained the hourly solar radiation record from SoDa for a year and developed a code to identify days with high solar radiation. The code showed that daily average solar hours with high radiation were 7 h, corresponding to 705 W/m^2 average irradiances for Al-Qatrana.

Thermal energy collected from the receivers is transported and exchanged through heat exchangers, where the high performance of the HTF favors high thermal conductivity, specific heat capacity, and density. High thermal conductivity supports effective heat transfer from the absorber to the SHE1, and a high specific heat capacity and density can increase heat flux with the minimum mass flow rates since the working temperature before the CC is higher than 300 °C.

To satisfy these requirements, we selected solar salt ($60NaNO_3$-$40KNO_3$) based on the studies of [43]. The HTF mass flow rate range per tube is (0.8–2) kg/s, as seen in [44]. Note that solar salt has a greater heat capacity and higher thermal conductivity than oil-based HTFs, whose properties are considered functions of the operating temperatures and pressures in each stream of the cycle instead of fixed properties [36], to reflect a change in the operating temperature. The methodology used in modeling the CSP field and the heat losses was adopted from [44]. Appendix A provides the equations used in modeling the CSP field and its heat losses.

3.4. Modeling of ACU

The ACU works in a single-effect stage with a mixture of LiBr and H_2O as the working fluid and refrigerant, respectively, which is more environmentally friendly than ammonia/H_2O. The cycle has a simpler configuration than double- and triple-effect stages, requiring lower maintenance and cost. After delivering part of the thermal heat in SHE1, the remaining heat from the HTF will be used to operate the generator also known as SHE2. The relatively high operating temperature, T_{so} > 370 °C, has been justified by Talbi and Agnew [37], who used diesel engine waste heat with a running temperature above 370 °C to drive an ACU. In this work, the ACU is controlled by the amount of cooling required by the GT, i.e., the amount of energy transferred from the inlet air until the temperature reaches 5 °C before entering the compressor.

The properties for each component in ACU were fixed; therefore, the refrigerant's mass flow rate is considered a variable controlled by cooling load using energy conservation equations. Also, depending on the cooling load, the required heat input thermal energy entering the generator changes, leading to different outlet temperatures for the HTF in SHE2. The properties of the H_2O refrigerant were obtained by each stream's indicated temperature and quality. Modeling the ACU was carried out using the methodology reported in [45], where the effect of relative humidity was negligible because the ACU cools the air before entering the compressor by sensible cooling, which means no water will be introduced to the system [7]. The power required by the absorption pump was identified as negligible. Constraints for operation [46] included the following: The system is assumed to operate under steady-state conditions. The refrigerant exits the condenser as a saturated liquid, the evaporator exits as a saturated vapor, the solution departs the generator and absorber as saturated liquids, and the water concentration in the LiBr/H_2O that exits the generator is fixed. Appendix A shows the adopted equations for the absorption system simulation.

3.5. Thermo-Environomic Modeling

Due to the current global warming trend and increasing air pollution, it is essential to evaluate the thermal effect of gas turbines on the environment. We include three major pollutants, CO, NO_x, and CO_2 (CO and NO_x as toxic and CO_2 as greenhouse gas [47]), in modeling natural gas [48] combustion to maximize fuel efficiency and minimize its environmental effects [12]. To make the thermo-environomic modeling relevant and effective to the gas turbine combustion system, semi-empirical correlations were employed as suggested by [35] and shown in Appendix A.

3.6. Overall Performance Analysis

The above model provides performance parameters on the combined parabolic trough collectors and absorption chilling unit (PACC). These parameters are fuel flow rate and thermal efficiency, the total generated power, and the specific fuel consumption. These parameters were estimated using the methodology reported in [33]. Appendix A provides all equations to calculate these performance parameters.

4. Results and Discussion

4.1. Validation of the Developed Model

The developed code was benchmarked against the available models of the PACC components (GT, HRSG, CSP, and ACU) using experimental and theoretical data in the literature [7,41,45]. However, our current integrated system is new and requires independent validation.

We applied the available literature values [49] to our conditions and conducted the following validation steps. The first step is to simulate the outputs of the case study investigated. Afterward, the results were benchmarked against the data reported in [30], which showed good agreement, with a maximum difference of 9.6% for the GT 75% load case, as shown in Table 2. Afterwards, separate codes were developed and benchmarked against the results reported in the literature for the ACU [7] and for the PTC [41].

Table 2. Validation of the developed models compared to the models reported in the literature.

GT		Power Generated at Full and Part Loads		
		Present Study	Ref. [30]	Relative Difference (%)
Load %	100%	268,828 (kW)	256,438 (kW)	4.83
	75%	211,608 (kW)	193,034 (kW)	9.62
HRSG		Heat Transferred at Full and Part Loads		
		Present Study	Ref. [30]	Relative Difference (%)
Load %	100%	133,829 (kW)	132,736 (kW)	0.82
	75%	112,068 (kW)	111,736 (kW)	0.30
ACU		Based on the Cooling Load (kW/ kg_{ref})		
		Present Study	Ref. [7]	Relative Difference (%)
q_{evap} (kW/kg_{ref})		2495 (kW/ kg_{ref})	2316 (kW/ kg_{ref})	7.73
PTC		Collected Heat Considering Ambient Temperature and Heat Loses		
		Present Study	Ref. [41]	Relative Difference (%)
$T_{a,avg}$ (°C)	100.6 (°C)	10.67 (W/m^2)	10.6 (W/m^2)	0.66
	149.1 (°C)	19.46 (W/m^2)	19.3 (W/m^2)	0.83
	196.7 (°C)	31.12 (W/m^2)	30.6 (W/m^2)	1.70
	245.8 (°C)	46.82 (W/m^2)	45.4 (W/m^2)	3.13
	293.3 (°C)	66.11 (W/m^2)	62.9 (W/m^2)	5.10

This can be considered a good validation. After gaining confidence in the developed subsystem codes, these codes were integrated with the previously validated power plant code to calculate the performance of the proposed system.

4.2. Design Point Calculations

After integrating the three (GTCC, PTC, and ACU) subsystems, we selected a simple design to evaluate against [7] the power augmentation, efficiency enhancement, fuel reduction, and SFC decrease with an EES code. From the exhaust temperature stated in Table 1, the TIT was found to be 1145.8 °C, r_p = 11.3, T_a = 36 °C, the average annual direct solar irradiation G_b = 705 W/m^2 (as justified in Section 3.3), the HTF flowrate (m_s) was 1.505 kg/s, 10 Col_s, and 420 Col_r.

When the operating parameters are selected, the code can be integrated. Table 3 displays the state points and thermodynamic properties for the system at the necessary design calculations. A comparison between the novel design and the conventional GTCC is detailed in Table 4 for the system's impact and advantages. When the novel cascaded solar system is integrated, the compressor inlet temperature drops by 5 °C, and the compressor work cuts back by 10.8%, but unfortunately, the compressor outlet temperature drops as a negative performance. To overcome this negative performance, SHE1 would increase the compressed air temperature by 41.2% to decrease the amount of fuel consumed in the system by 10.5% compared with the conventional power plant. This is accompanied by a significant reduction in pollutant emissions, as follows: CO_2 4.21 kg/s, CO 0.0257 kg/s, and NO_x 0.2778 kg/s. However, this reduction in fuel consumption results in reducing the gases' mass flow rate through the gas turbine, hence slightly reducing its generated power by 1.69%.

Table 3. State point thermodynamic properties along with the PACC system.

State Point	Fluid	Temperature (°C)	Pressure (kPa)	Mass Flow Rate (kg/s)
a	Air	36	100	2 × 432.6
1	Air	5	100	2 × 432.6
2	Air	358.1	1130	2 × 432.6
2a	Air	505.8	1107	2 × 432.6
3	Gas	1145.8	1085	2 × 440.7
4	Gas	569	101	2 × 440.7
5	Gas	218.3	101	881.4
6	Gas	175.8	101	881.4
7	Gas	115	101	881.4
8	Steam	551	7620	116
9	Steam	219.8	500.1	116
10	Steam	205.6	500.1	17.2
11	Steam	217.9	500.1	133.2
12	Steam	57.93	18.1	133.2
13	Water	57.5	17.74	133.2
14	Water	57.6	531.1	133.2
15	Water	57.6	531.1	133.2
16	Water	153.4	520.7	17.2
17	Water	153.4	520.7	116
18	Water	154.8	8248	116
19	Gas	514.4	101	881.4
20	Gas	478.6	101	881.4
21	Gas	301.8	101	881.4
22	Gas	216.1	101	881.4
23	Steam	153.4	510.3	17.2
24	Steam	295.8	8086	116
25	Steam	295.8	7928	116
26	Steam	370.8	7772	116
36	Steam	97	40.2	12.32
37	Water	76	40.2	12.32
38	Water	2	0.706	12.32
39	Steam	2	0.706	12.32
40	$LiBr/H_2O$	55	0.706	71.86
41	$LiBr/H_2O$	57	40.2	71.86
42	$LiBr/H_2O$	103	40.2	71.86
43	$LiBr/H_2O$	82	40.2	59.53
44	$LiBr/H_2O$	41	40.2	59.53
45	$LiBr/H_2O$	40	0.706	59.53
s_i	Solar Salt	484.8	1000	632.1
s_o	Solar Salt	372	1000	632.1
s_{oo}	Solar Salt	346.9	1000	632.1

Table 3. *Cont.*

State Point	Fluid	Temperature (°C)	Pressure (kPa)	Mass Flow Rate (kg/s)
$w_{1,in}$	Water	36	100	4632
$w_{1,out}$	Water	51	100	4632
$w_{2,in}$	Water	36	100	347.7
$w_{2,out}$	Water	56	100	347.7
$w_{3,in}$	Water	36	100	938.9
$w_{3,out}$	Water	46	100	938.9

Table 4. Difference in the performance parameters between the proposed system and Al-Qatrana plant at the design point conditions.

Performance Parameter	Al-Qatrana	Proposed System	Relative Difference [%]
Generated power [MW]	402.72	430.39	6.87
Thermal efficiency [%]	47.26	56.45	19.45
Fuel consumption [kg/s]	17.28	15.46	−10.53
SFC [$\times 10^{-5}$ kg/kW]	4.29	3.59	−16.32

4.3. Variation Impact of the Operating Parameters on the Performance of the System

The impact of the variation in operating parameters on the system's overall performance using the spider diagrams used in [50] is investigated in this section. Since ambient conditions influence the system, the impact of solar radiation, air inlet temperature, and the impact of operating parameters on the GTCC, namely TIT and r_p, were studied. Also, the main parameters to drive the PTC, which are m_s in each absorber tube, Col_r, and Col_s, were studied. Table 5 shows the operating ranges for these variables along with verification references. A wide range of operations will help us better understand the system's behavior for Al-Qatrana PP for other GTCCs applications. Table 6 summarizes the cooling load and heat input given by the ACU and the PTC, as well as the heat transfer coefficients of the ACU components.

Table 5. Operating parameters' acceptable ranges.

Operating Variable	Operation Range	References
Ambient temperature, T_a [°C]	15–45	[7]
Direct solar irradiation, G_b [W/m^2]	500–1050	[41]
Turbine inlet temperature, TIT or T_3 [°C]	1120–1350	[51]
r_p	7–13	[52]
m_r [kg/s]	0.8–2	[44]
Col_r	380–430	[7]
Col_s	8–13	[52]

Ambient temperature and incident solar irradiation are two operating parameters that can be controlled by selecting the location of the GTPP and operating hours by evaluating one parameter at the time and keeping the other constant. Figure 8 illustrates the following three different performances, (a) W_{net}, (b) η_{th}, and (c) SFC, all under the following conditions: T_a, G_b, Col_r, the Col_s, the HTF mass flow rate (m_r), TIT, and r_p of the GT.

Table 6. Specifications for the ACU and PTC fields.

Specifications	Value
ACU cooling load, Q_{CL} [MW]	26.94
PTC heat input, Q_{HI} [MW]	161.45
ACU generator heat transfer coefficient, $U_{ACU,Gen}$ [kW/m^{2}K]	1.3 [53]
ACU condenser heat transfer coefficient, $U_{ACU,Con}$ [kW/m^{2}K]	0.5 [53]
ACU evaporator heat transfer coefficient, $U_{ACU,Eva}$ [kW/m^{2}K]	1.1 [53]
ACU absorber heat transfer coefficient, $U_{ACU,Abs}$ [kW/m^{2}K]	0.8 [53]
ACU heat exchanger heat transfer coefficient, $U_{ACU,HE}$ [kW/m^{2}K]	0.7 [53]
SHE1 heat transfer coefficient, $U_{ACU,SHE1}$ [kW/m^{2}K]	0.3 [54]

These non-dimensional results were calculated by dividing the values of the varying operating and performance parameters over the corresponding design values while keeping the inlet compressor temperature at 5 °C to provide the lowest energy consumption in the compressors. When the ambient temperature increases, the cooling load would increase, resulting in a decrease in $T_{s,oo}$, causing T_{si} to decrease and, therefore, lowering the useful solar heat input into the system from SHE1 and sending more fuel to maintain constant GT inlet temperature. A higher amount of fuel would cause a relatively small increase in the turbines' work, as shown in Figure 8a. By contrast, Figure 8b shows a drop in thermal efficiency with the raise in the ambient air temperature, while Figure 8c illustrates a proportional relation between the SFC and the ambient air temperature where the resulting surge in fuel consumption outweighs the increased power explained earlier, resulting in the noted behaviors. The result is that a 10% increase in ambient air temperature would increase the cooling load by 11.6%, decrease T_{soo} by 0.92%, decrease T_{si} by 0.6%, and increase fuel consumption by 0.45%, hence increasing power by 0.04%, decreasing η_{th} by 0.44%, and increasing the SFC by 0.42%.

Figure 8a–c show the variation in solar radiation as a function of the W_{net}, η_{th}, and SFC, which indicate that the power and SFC decrease while the thermal efficiency grows as G_b increases. That is because, with a higher amount of solar radiation, the HTF temperature exiting the PTC field is increased due to the higher amount of energy absorbed in the PTC; the thermal energy associated with elevated temperature in the HTF is transferred to the compressor air that will be combusted in the combustion chamber. Since the TIT is fixed, the required fuel to be injected will be lower (because T_{si} is already high). The power output will decrease due to the lower amount of hot gases entering the turbines (since fuel is reduced). Overall, thermal efficiency will increase, and SFC will reduce because the percentage decrease in fuel consumption is higher than the decrease in power output.

Furthermore, a sensitivity analysis was conducted to show that a 10% increase in solar radiation increases T_{si} by 3.26%. Specific results included the findings that the compressed air temperature (T_{2a}) was increased by 3.4%, hence decreasing the fuel consumption by 2.5%, causing a reduction in the turbine power by 0.12% and, therefore, power reduction by 0.23%, thermal efficiency improvement by 2.39%, and SFC reduction by 0.023%. The hot gases coming from the GT are reduced due to a decrease in fuel consumption, influencing the performance of the HRU, especially the STs, and the ST cycle's net power, which was altered by a 0.19% reduction when a 10% increase in G_b occurs.

Figure 8a–c also illustrate the influence of m_r variation on the performance parameters of the PP (W_{net}, η, SFC) and show that increasing the value of m_r will not affect performance. When applying a higher m_r, while the solar flux on the PTCs is fixed, T_{si} is expected to decrease due to energy conservation. Solar heat input remains constant over the variation in m_r. Consequently, the mass flow rate of the fuel, the power output, thermal efficiency, and SFC remain constant, while a 10% increase in m_r lowers the T_{si} by 0.67% and keeps the solar heat input constant at 161.4 MW.

Afterward, the effects of varying Col_r on the overall performance parameters (W_{net}, η, and SFC) were estimated. Increasing the number of collectors increased m_r while keeping its temperature constant, which led to a higher amount of useful solar heat input into the system, causing a reduction in fuel intake. The power augmented stayed constant since, as stated earlier, the ambient temperature was reduced to 5 °C. However, the reduction in fuel consumption is more significant with η and SFC, as η increased and the SFC decreased. The total net solar heat input would increase by 9.9%, with a 10% increase in Col_r. Therefore, T_{2a} would increase by 3.4%, leading to a 2.6% reduction in fuel consumption, resulting in a 0.22% reduction in power, a 2.3% relative increase in efficiency, and a 2.3% decrease in SFC.

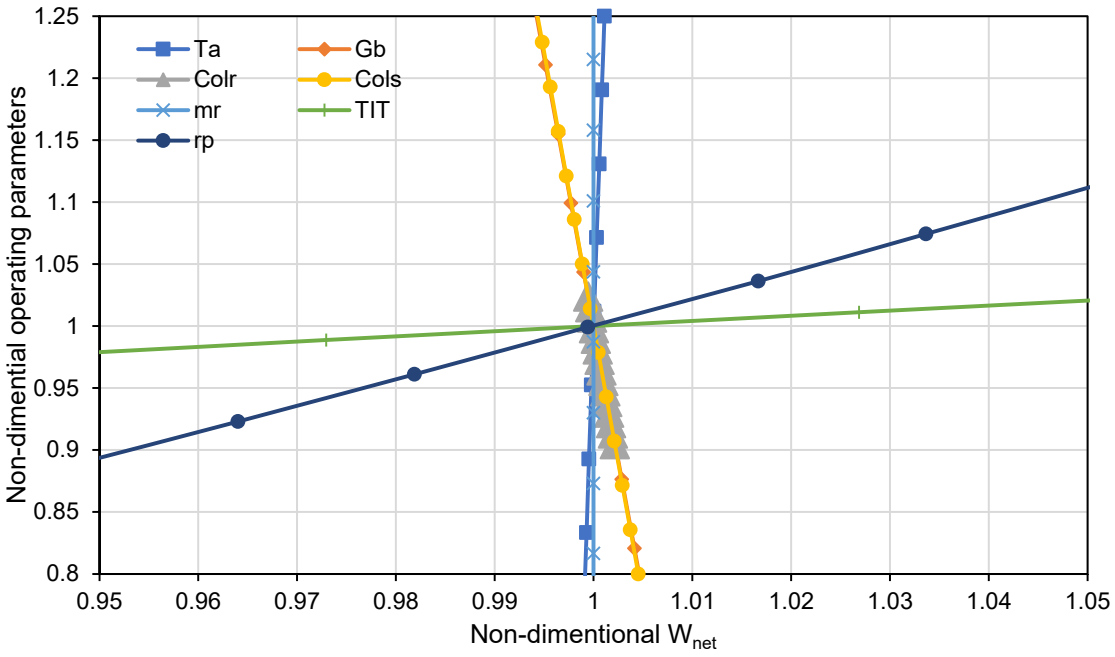

(**a**)

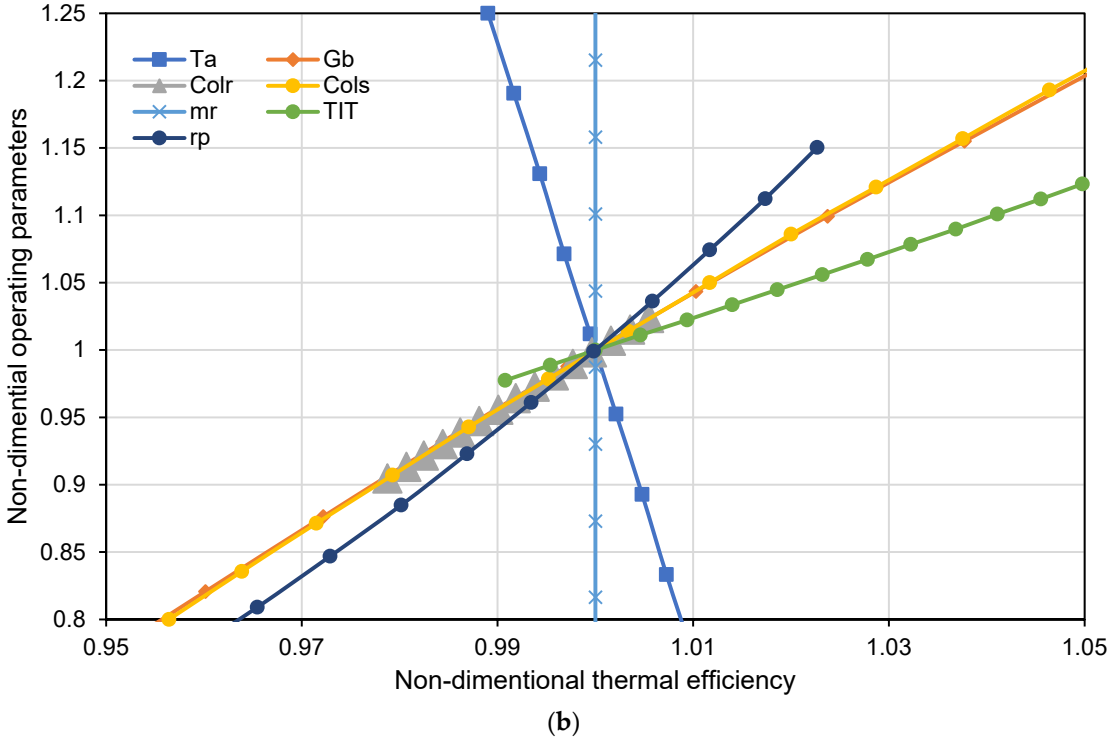

(**b**)

Figure 8. *Cont.*

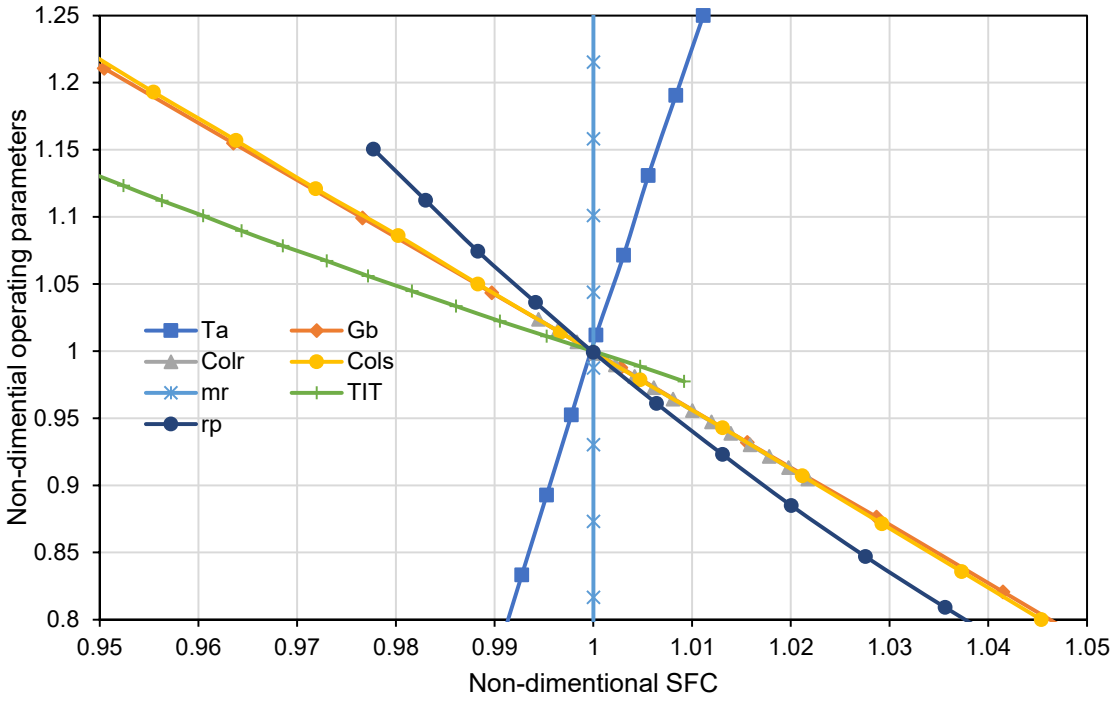

(**c**)

Figure 8. The impact of the operating parameters on (**a**) output power, (**b**) thermal efficiency, and (**c**) SFC.

Moreover, the effects of varying Col_s on the performance parameters (W_{net}, η, SFC) were estimated; it was found that increasing Col_s increased the temperature of the HTF coming out from the PTC field. Hence, more solar power is introduced, causing the compressed air temperature to increase and, therefore, the mass flow rate for the fuel to decrease. When the mass flow rate of the fuel is reduced, thermal efficiency will increase, while the power and SFC will decrease. A 10% increase in Col_s would cause the following: a 3.36% increase in T_{2a}, 2.5% increase in m_f, 0.2% decrease in power, 2.3% increase in efficiency, and 2.3% decrease in SFC.

To study the system's behavior under different operating loads, the variation for operating parameters TIT and r_p were studied since the GT loads usually change depending on the power demand. Accordingly, the TIT and r_p change. Figure 8a–c show that increasing TIT would increase the power output and thermal efficiency and decrease the SFC because the higher temperature allowed in the turbine would generate more expansion in the combustion product gases and release more energy that is transformed into mechanical power, increasing the power output and lowering the SFC. Note that although the mass flow rate of the fuel increased, the thermal efficiency still increased because the power output increase due to the higher TIT outweighs the increase in the fuel's mass flow rate. Sensitivity analysis showed that a 10% increase in TIT results in a 20% increase in fuel consumption, a 25% increase in power generation, a 4.1% rise in efficiency, and a 3.9% reduction in SFC. On the other hand, increasing r_p while holding the rest of the operating parameters fixed would increase both the power generation rate and thermal efficiency and decrease the SFC. A 10% increase in r_p would increase both the power and efficiency by 4.4% and 1.5% and decrease SFC by 1.5%.

Figure 9a,b present the influence of different operating parameters on the CO and NOx production rate measured in gram/second per kg of fuel. Measuring the species production rate (emission rate) per kg of fuel can help us mitigate the effects of the fuel consumed on the emission rate and, therefore, is important for environmental and pollution analysis. As T_a increases, the cooling load increases in ACU, dragging more heat from HTF and decreasing the inlet temperature of air (2a) before it enters the CC, slightly reducing the

adiabatic flame temperature. As a result, the production rate of CO per kg of fuel increases in a small amount. The production rate of NO_x per kg of fuel decreases, as seen in A57, since the adiabatic flame temperature decreases.

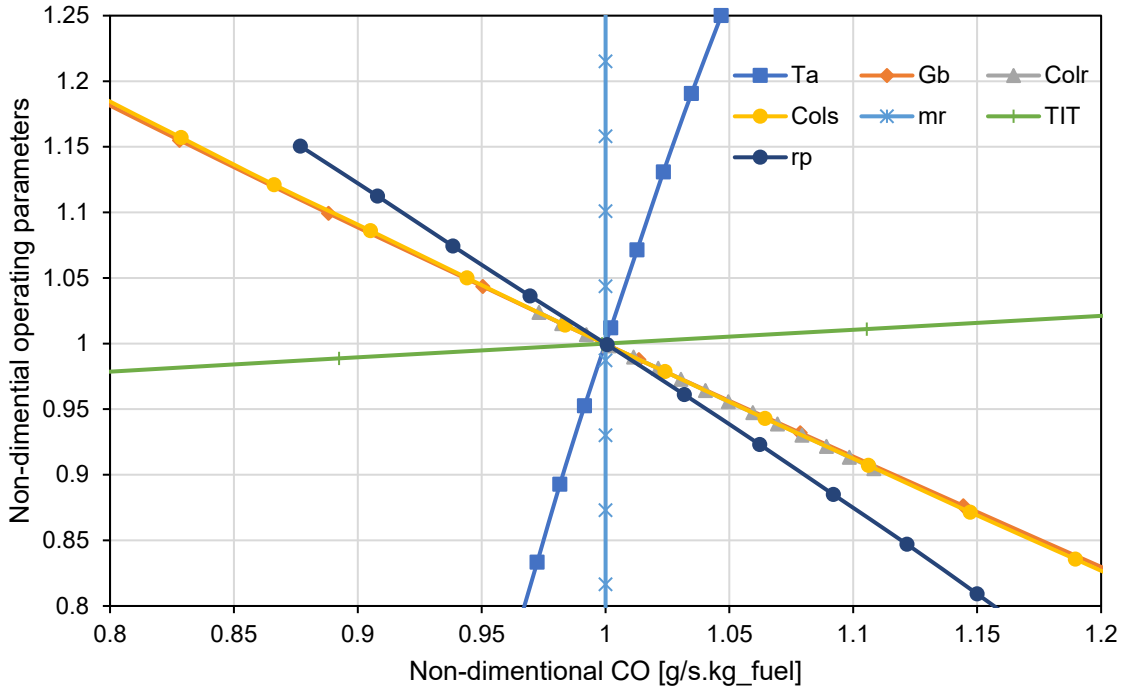

(**a**)

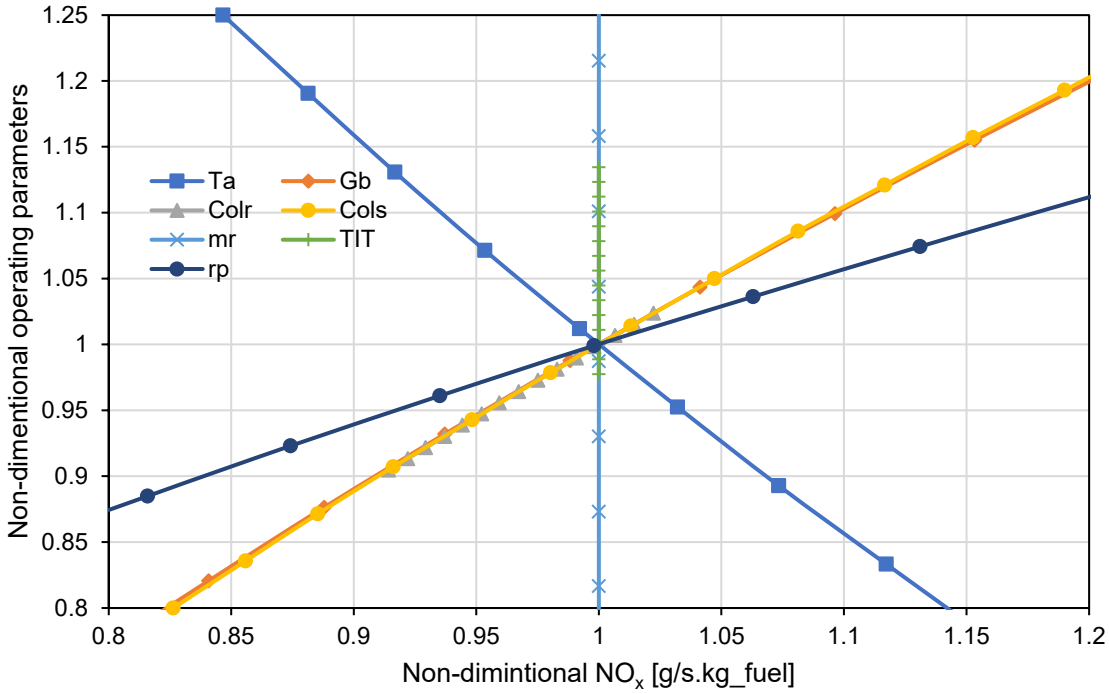

(**b**)

Figure 9. The impact of the operating parameters on (**a**) CO emissions and (**b**) NOx per kg fuel.

A 10% increase in T_a increases the CO emission rate per kg of fuel by 0.65%, decreasing the NO_x emission rate per kg of fuel by 2.76%. Similarly, an increase in G_b, Col_r, or Col_s, will increase the thermal energy of the high-temperature fluid. As a result, T_{2a} increases. This

rise in the air temperature increases the adiabatic flame temperature inside the combustion chamber, helping to decrease CO emissions per kg of fuel and increasing the NO_x emission per kg of fuel. A 10% increase in G_b decreases the CO emission rate per kg of fuel by 6.41% but increases the NO_x emission rate per kg of fuel by 7.5%. Similarly, a 10% increase in Col_s would decrease the CO emission rate per kg of fuel by 7.64% and increase the NO_x emission rate per kg of fuel by 8.09%. The same 10% increase in Col_r decreases the CO emission rate per kg of fuel by 9.32% and increases the NO_x emission rate per kg of fuel by 8.89%.

The emission of CO and NO_x per kg of fuel remains independent of m_r because it would cause no change to the total thermal energy available for heat exchange at SHE1 and makes no impact on the thermodynamic condition of the combustion chamber to alter the emission rates. Among all the operating parameters, TIT has the most significant influence on CO emission per kg of fuel. A 10% increase in TIT would increase CO emission rate per kg of fuel by 107.17%. An increase in TIT requires more fuel to be injected in the CC, thus increasing the fuel–air equivalence ratio. As a result, the adiabatic flame temperature drops, and CO emission per kg of fuel also increases dramatically.

The NO_x emission per kg of fuel is independent of TIT and depends only on stoichiometric (adiabatic) flame temperature under little influence of the fuel–air equivalence ratio. An increase in r_p increases air pressure entering the combustion chamber at point 2a, which reduces the CO emission per kg of fuel. By contrast, the same scenario increases the NO_x emission per kg of fuel based on A57. A 10% increase in r_p, would decrease the CO emission rate per kg of fuel by 2.83% and increase the NO_x emission rate per kg of fuel by 15.78%.

Figure 10 shows the nondimensionalized operating parameters' effect on the nondimensionalized emission rate of (a) CO, (b) NOx, and (c) CO_2. All seven operational parameters (T_a, G_b, Col_s, Col_r, m_r, TIT, and r_p) create a similar impact on CO and NOx emission rate as they did on the CO emission rate per kg of fuel and NOx emission rate per kg of fuel, because trend lines of respective operating parameters are identical in Figure 9a,b and Figure 10a,b, whereas TIT differently influences NOx emission rate per kg of fuel. Comparison between Figures 9b and 10b shows that the NO_x emission rate per kg of fuel remains constant with increasing TIT.

A higher TIT requires more fuel to be injected into the CC, therefore increasing the NO_x flow rate. The rate of CO_2 emission is directly proportional to the amount of fuel injected into the combustion chamber. Variation in the emission rate of CO_2 (kg/s) based on the seven different operating parameters is shown in Figure 10c. When T_a increases, the ACU's thermal load increases, pulling more heat from the HTF and decreasing T_{2a} at the combustion chamber inlet because less heat is available for heat exchange at SHE1. To keep the TIT constant, fuel input into the combustion chamber increases the CO_2 emission rate. Thus, a 10% increase in T_a increases the CO_2 emission rate by 0.20%.

Meanwhile, with an increase in G_b or Col_r or Col_s, the thermal energy available for heat exchange at SHE1 increases, which results in an increased T_{2a} of air into the combustion chamber. This requires less fuel to keep the TIT fixed, and the CO_2 emission rate decreases. A 10% increase in G_b causes a drop in the CO_2 emission rate of 1.69%. Similarly, a 10% increase in Col_r reduces the CO_2 emission rate by 2.21%, whereas 10% increase in Col_s decreases the CO_2 emission rate by 1.91%.

The emission rate of CO_2 remains independent of m_r because it would make no change to the total thermal energy available for heat exchanger SHE1, and fuel injected into the CC remains unchanged. Increasing the air temperature at the outlet of the CC requires more fuel, thus increasing TIT and resulting in a significant increase in the CO_2 emission rate. A 10% increase in TIT increases the CO_2 emission rate by 20.53%, while the same 10% increase in r_p increases the CO_2 emission rate by 2.62%.

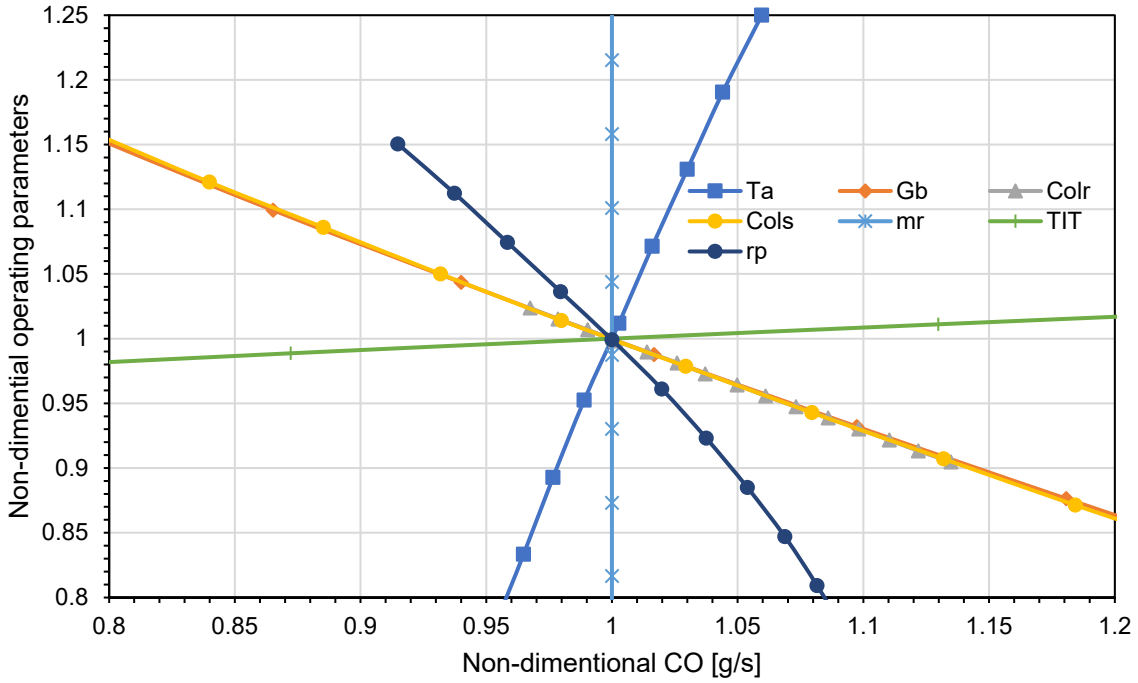

(**a**)

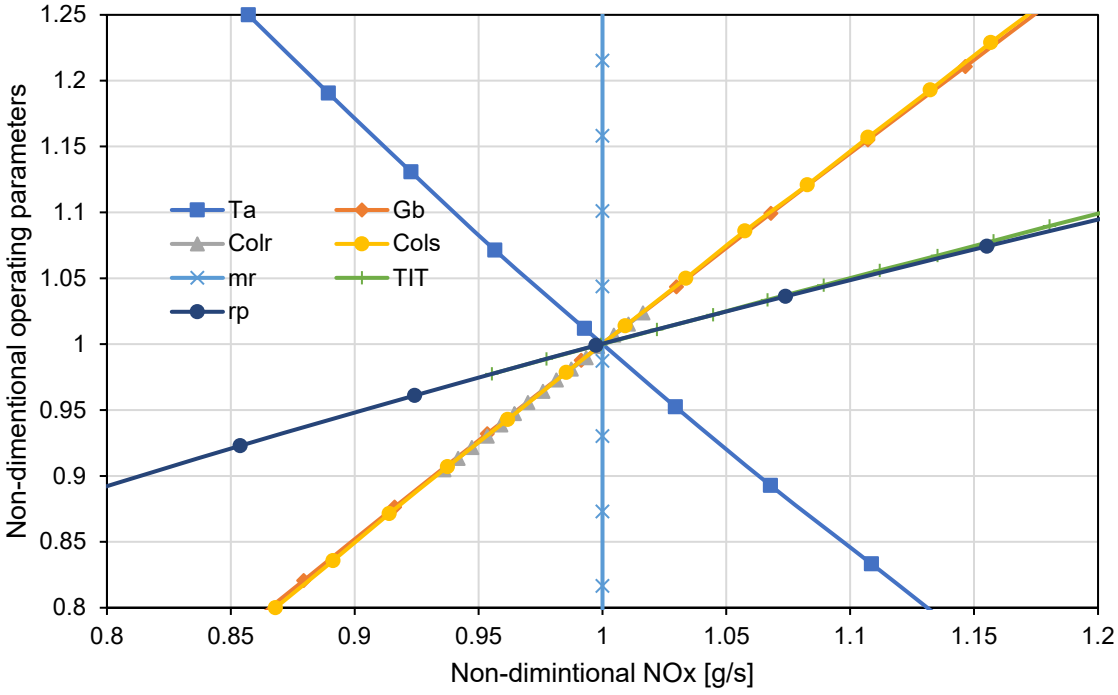

(**b**)

Figure 10. *Cont.*

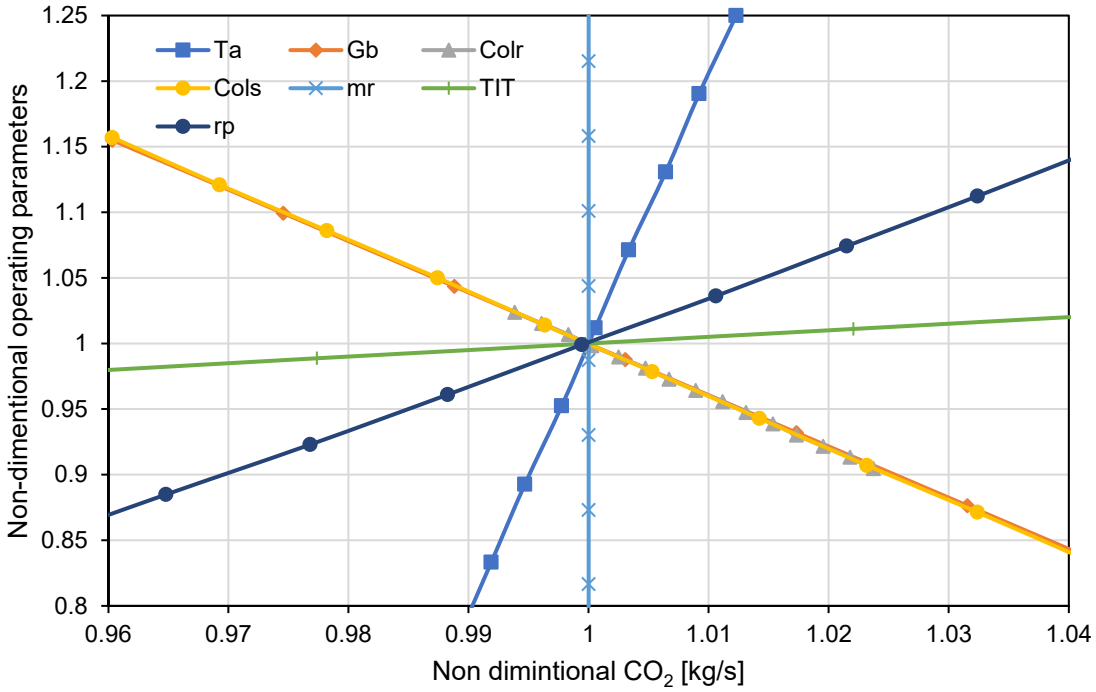

(**c**)

Figure 10. The impact of the operating parameters on the (**a**) CO emissions, (**b**) NOx emissions, and (**c**) CO_2 emissions.

4.4. The First and Second Laws of Thermodynamics Optimization

Optimization studies have been conducted on the novel integration to identify the optimal performance based on the first and second laws of thermodynamics [55]. Figure 11 shows a summary of the optimization's main results.

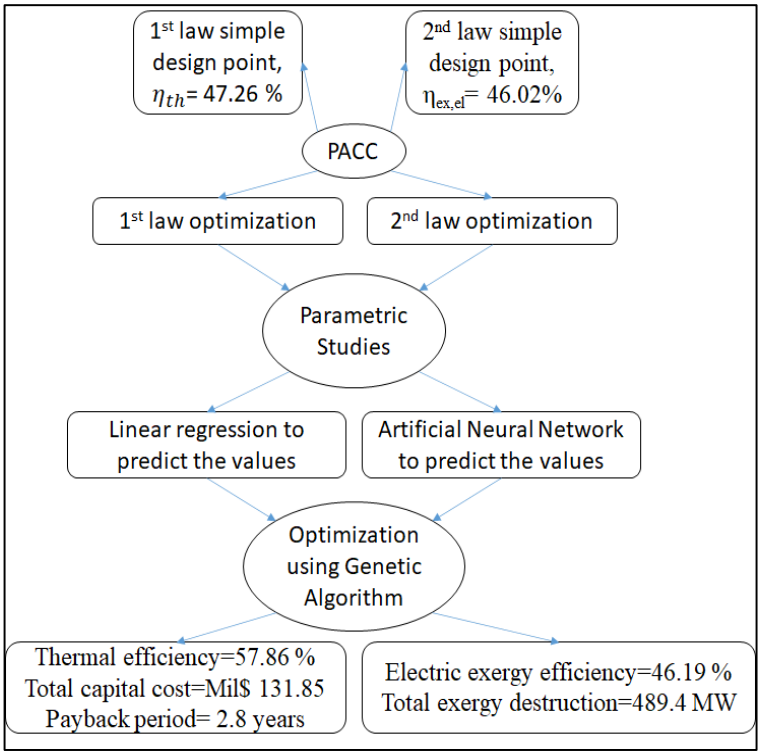

Figure 11. Flow chart for the optimization process.

Optimization of the first law consisted of maximizing the thermal efficiency of the integrated cycle while minimizing the capital cost of the PTC/ACU [33]. Thermal efficiency was selected as the main parameter in the optimization to evaluate the power plant's performance. Because it accounts for obligatory fuel consumption while considering power output instantaneously, this optimizes the plant's performance with regard to its efficiency, ensuring optimal, efficient fuel consumption, whereas the capital cost was chosen to ensure the economic viability of the proposed system, which determines if the proposed installment is realistic.

Based on the parametric study, two highly accurate polynomial equations were formulated using linear regression to implement them in the optimization process. These formulas are employed to estimate the values of the thermal efficiency and the capital cost, where the operating parameters are the independent variables. These formulas were employed in a Genetic Algorithm-based multi-objective optimization method using MATLAB to calculate the best performance in terms of the optimum value of first law efficiency and reasonable total cost. The results indicated that the optimum thermal efficiency would be 57.9%, corresponding to a capital cost value of 131.85 million USD. Additionally, the work was extended to conduct the payback period of the PTC/ACU. The economic analysis was based on savings from fuel revenues, increased power generated, social costs, and capital costs. Based on the optimum values of the capital cost and thermal efficiency, the payback period was found to be 2.8 years, which implies that the novel cycle is feasible.

Optimizing the second law consisted of minimizing overall exergy destruction while maximizing electrical exergy efficiency [55]. ANN was used to build the multi-objective optimization in MATLAB using the data obtained from a parametric study to develop the ANN. The input data to the ANN were a combination of different ranges of Col_s, Col_r, m_r, TIT, r_p of the GT, and the temperature difference in the proposed ACU condenser. Same as first law optimization, the Genetic Algorithm optimization approach was also used to investigate the optimum values from the second law's point of view. The results show that the optimal system can achieve 46.2% electric exergy efficiency with 489 MW overall exergy destruction.

4.5. Evaluation of the Proposed System's Improvements

Finally, Table 7 briefly compares different modifications proposed in the literature to enhance the performance of GT and GTCC PP by cooling the air entering the compressor, integrating solar energy, and adopting secondary systems.

Table 7. A brief comparison of different enhancements on GT and GTCC PPs presented in the literature.

Ref.	Summary	Key Pros	Key Disadvantage	Key Findings
This study	Combined cycle power plant incorporated with compressed air heater and air-cooling system, both operated by solar energy.	• Boosting the generated power. • Reducing the power plant fuel consumption.	• Intermittent of renewable energy.	Increasing efficiency from 47.26% to 61.1%.
Bellos et al. [52]	Gas turbine combined with PTC that directly heats the compressed air of the GT.	• Decreasing fuel consumption and evaluating the pressure drop in the turbine	• The HTF is the compressed air that causes larger PTC.	Fuel is saved by 64%.

Table 7. *Cont.*

Ref.	Summary	Key Pros	Key Disadvantage	Key Findings
Darwish Ahmad et al. [7]	GTCC with hybrid air-cooling system with PTC for generating steam.	• Utilizing waste heat. • Boosting generated power. • Improving efficiency.	• Introducing a large number of components. • Additional fuel consumption by IAC.	Increasing the efficiency to 52%.
Najjar et al. [24]	Combined gas turbine with two propane cycles.	• Utilizing waste heat. • Boosting generated power. • Improving efficiency.	• Insufficient amount of waste heat. • Additional fuel consumption by IAC.	Increasing the efficiency from 28.5% to 41.3%.
Yazdi et al. [35]	Various IAC technologies integrated with various GTs.	• Boosting generated power. • Improving efficiency.	• Additional fuel consumption by IAC. • Sensitivity to humidity while fogging is being used.	Increasing the efficiency by 5.5–5.8%.
Dashyebayaz and Najafabad [56]	Integrating NG pressure drop station with GT.	• Improving efficiency.	• Hazardous method due to releasing NG.	The efficiency was enhanced by 2.5%.
Alizadeh et al. [57]	Combined GTCC power plant with CSP.	• Utilizing clean energy. • Boosting generated power. • Improving efficiency.	• Limited therminol maximum temperature (400 °C).	Increasing the efficiency from 28.4% to 44%.
Avval et al. [19]	GTPP integrated with air preheater.	• Utilizing waste heat. • Reducing fuel consumption. • Improving efficiency.	• Waste heat was limited.	Increasing the exergy efficiency to 44%.
Baghernejad and Yaghoubi [58]	GTCC with CSP.	• Utilizing clean energy. • Boosting generated power. • Improving efficiency.	• Vulnerable to the variation in air temperature.	Increasing the exergy efficiency 47%.
Amelio et al. [59]	GTCC integrated with air-based PTC.	• Utilizing clean energy. • Reducing fuel consumption. • Improving efficiency.	• Significant large number of PTCs.	Increasing the efficiency from 51.4% to 60.9%.
Yari and Mahmoudi [60]	Driving GT combined with two Organic Rankine Cycles (ORCs) by Helium reactor.	• Utilizing waste heat. • Boosting generated power.	• Require a unique power source. • Hazardous.	Increasing the efficiency by 3%.
Ebrahimi and Moradpoor [61]	Integrated solid oxide fuel cell, mGT, and ORC.	• Utilizing waste heat. • Improving efficiency	• Works for micro-GTs.	Increasing the efficiency by up to 61%.
Schwarzbözl et al. [62]	Solar gas turbine.	• Utilizing clean energy. • Reducing fuel consumption. • Improving efficiency.	• Require a larger number of solar towers.	Increasing the efficiency from 40% to 50%.

5. Conclusions

This study investigated the integration of a combined cogeneration cycle system with PTC cascaded with an inlet air cooling system to enhance the performance of a combined cycle power plant under normal and rough ambient conditions. We developed our system model to utilize solar power to drive a cascaded solar heat exchanger. The system model has been shown to reduce the compressor inlet's ambient temperature to 5 °C. Although this reduction results in a drop in the combustion chamber inlet temperature, which causes a rise in fuel consumption, the novel integration can counter this change via solar hearing. A simulation-constructed approach was applied to validate predictions from these models with actual plant and literature data. It evaluated the cooling load impact of the ACU and the solar heat input on the system's total power generation, thermal efficiency, and SFC. The specific results from this study can be summarized as follows:

(1) The method proposed in this study assesses the overall performance of the gas turbine system, which can be applied to evaluate other existing and future GT powerplants.
(2) A cascaded solar power system was proposed to improve the system's overall performance, increase the power generation at the design point by 6.87%, and improve thermal efficiency by 19.5% with a 10.53% reduction in fuel consumption.
(3) The ACU successfully lowered the ambient temperature to 5 °C using the available solar power that drives the generator (solar heat exchanger number 2), resulting in the compressors' lowest consumed power.
(4) Utilizing solar power in solar heat exchanger number 1 saved the maximum amount of NG fuel input by solving two problems: the conventionally high amounts of fuel required for generating power in the GTs and the rise in the temperature difference caused by the inlet air cooling.
(5) The effect of each of the seven main operating parameters on the overall performance of the system was quantified and explained.

Future studies should address the remaining aspects of the system's feasibility, such as real-time dynamic responses with regard to the variables of the grid-like voltage, active power, and reactive power dissipation. Additionally, since the integration of this system was investigated for larger-scale applications, power plants in this case, it would be interesting to test the feasibility of such integrations on much smaller scale systems that involve air compression and combustion.

Author Contributions: A.M.A.: Conceptualization; Data curation; Formal analysis; Investigation; Methodology; Resources; Software; Validation; Roles/Writing—Original draft; Writing—Review and editing. A.D.A.: Conceptualization; Data curation; Formal analysis; Investigation; Methodology; Resources; Software; Validation; Roles/Writing—Original draft; Writing—Review and editing. B.B.S.: Formal analysis; Software; Roles/Writing—original draft. Y.M.M.: Writing—Original Draft, Writing—Review and Editing. L.A.-G.: Formal analysis, Resources; Software; Validation; Writing—Original Draft, Writing—Review and Editing. N.K.A.: Conceptualization; Funding acquisition; Investigation; Project administration; Resources; Supervision; Roles/Writing—Original draft; Writing—Review and editing. K.S.: Conceptualization; Data curation; Formal analysis; Funding acquisition; Project administration; Resources; Supervision; Roles/Writing—Original draft; Writing—Review and editing. All authors have read and agreed to the published version of the manuscript.

Funding: This study was sponsored by the University of Kentucky IR4TD research fund.

Institutional Review Board Statement: Not applicable.

Informed Consent Statement: Not applicable.

Data Availability Statement: The data presented in this study are available on request from the corresponding author.

Acknowledgments: University of Kentucky's IR4TD members for their valuable comments and discussion.

Conflicts of Interest: The authors declare no conflict of interest.

Abbreviations

ACU	Absorption chilling unit
CC	Combustion chamber
CCGT	Combined-cycle gas turbine
Col_r	Number of collectors in row
Col_s	Number of collectors in series
CSP	Concentrated solar power
CSS	Cascade solar system
CWHR	Cascaded waste heat recovery
EES	Engineering equation solver
G_b	Solar irradiation
GTs	Gas turbines
GTCC	Gas turbine-combined cycle
GTPPs	Gas turbine power plants
HP	High-pressure heat recovery steam generator
HPEC	High-pressure economizer
HPSH	High-pressure superheater
HPST	High-pressure steam turbine
HRSG	Heat recovery steam generation
HRU	Heat recovery unit
HTF	Heat transfer fluid
IAC	Inlet air cooling
ISCCs	Integrated solar combined cycle power plants
LFCs	Linear Fresnel collectors
LHV	Lower heating value
LP	Low-pressure heat recovery steam generator
LPEV	Low-pressure evaporator
LPST	Low-pressure steam turbine
MCU	Mechanical chiller unit
m_r	HTF mass flow rate
NG	Natural gas
P_a	Ambient pressure
PACC	Integrated GTCC combined with PTC/ACU
PPs	Power plants
PTCs	Parabolic trough collectors
r_p	Pressure ratio
SFC	Specific fuel consumption
ST	Steam turbine
T_{2s}	Compressed air temperature
T_a	Ambient temperature
TIT	Turbine inlet temperature
T_{pz}	Adiabatic flame temperature (K)
$T_{s,oo}$	Inlet temperature of HTF into PTC
T_{si}	Outlet temperature of HTF from PTC
T_{so}	Operating temperature
T_{st}	Stoichiometric temperature (K)
W_{net}	Overall power
Greek letters	
η_{th}	Thermal efficiency
Subscripts	
1–45	State points
CO	Carbon monoxide
CO_2	Carbon dioxide
H_2O	Water
LiBr	Lithium bromide
NO_x	Nitrogen oxides

Appendix A

Table A1. Modeling of the power plant components.

Module	Equation	Crucial Points	Equation Number
Gas turbine engine			
Air compressors [38]	$r_p = \frac{P_2}{P_1}$	The pressure at the compressor's outlet is estimated using r_p	(A1)
	$\eta_c = 1 - (0.09 + \frac{r_p - 1}{300})$	Compressor's efficiency (polytropic)	(A2)
	$(\frac{n_a - 1}{n_a}) = \frac{\gamma_a - 1}{\gamma_a \eta_c}$		(A3)
	$T_2 = T_1 (r_p)^{(n-1)/\mathrm{n}\ \eta_p}$	From (A1), (A2), and (A3), one can find air compressors temperature	(A4)
	$\dot{W}_c = \dot{m}_1 (h_2 - h_1)$	Power required for the compressors. At each defined state (i), the enthalpy was estimated using the libraries in EES	(A5)
Combustion chamber [38,63–65]	$\dot{m}_{2a} h_{2a} + \dot{m}_f LHV = \dot{m}_3 h_3 + (1 - \eta_{CC}) \dot{m}_f LHV$	Conservation of energy in the CC	(A6)
	$\dot{m}_3 = \dot{m}_1 + f\ \dot{m}_1$	Hot gases' mass flow rate	(A7)
	$f = \frac{\int_{T_1}^{T_3} C_{CG,3} \cdot dT - \int_{T_1}^{T_{2a}} C_a \cdot dT}{(LHV - \int_{T_1}^{T_3} C_{CG,3} \cdot dT)\eta_{CC}}$	Fuel-to-air ratio is calculated based on the energy balance given in (A6)	(A8)
	$C_{CG} = C_a + \frac{f}{1+f}\ (1.0887572 \times 10^3 - 1.4158834 \times 10^{-1} T + 1.9160159 \times 10^{-3} T^2 - 1.2400934 \times 10^{-6} T^3 + 3.0669459 \times 10^{-10} T^4 - 2.6117109 \times 10^{-14} T^5)$	Flue gas specific heat used in (A8)	(A9)
	$\lambda C_{x1} H_{y1} + (x_{O_2} O_2 + x_{N_2} N_2 + x_{H_2O} H_2O + x_{CO_2} CO_2 + x_{Ar} Ar) \rightarrow y_{CO_2} CO_2 + y_{N_2} N_2 + y_{O_2} O_2 + y_{H_2O} H_2O + y_{NO} NO + y_{CO} CO + y_{Ar} Ar$	General combustion reaction, where $y_{CO_2} = (\lambda * x1 + x_{CO_2} - y_{CO})$, $y_{N_2} = x_{N_2} - y_{NO}$, $y_{H_2O} = x_{H_2O} + \frac{\lambda * y_1}{2}$, $y_{O_2} = x_{O_2} - \lambda * x_1 - \frac{\lambda * y_1}{4} - \frac{y_{CO}}{2} - \frac{y_{NO}}{2}$, $y_{Ar} = x_{Ar}$, $\lambda = \frac{\eta_{fuel}}{\eta_{air}}$	(A10)
	$P_3 = P_{2a}\left(1 - \frac{\Delta P_{combustor}}{P_{2a}}\right)$	Estimation of the drop in the pressure across the CC	(A11)
Gas turbines [38]	$r_{GT} = \left(\frac{P_3}{P_4}\right)$	Pressure ratio of the turbines	(A12)
	$\eta_{\infty,GT} = 0.9 + \frac{r_{GT} - 1}{250}$	Polytropic efficiency of the gas turbine	(A13)
	$(\frac{n_g - 1}{n_g}) = \frac{\eta_{GT}(\gamma_g - 1)}{\gamma_g}$		(A14)
	$T_4 = T_3 (\frac{P_4}{P_3})^{\eta_{GT}(n_g - 1)/n_g}$	Turbine exhaust temperature	(A15)
	$\dot{W}_{GT} = \dot{m}_3 \int_{T3}^{T4} C_{CG,i} \cdot dT$	Generated power by hot gas expansion	(A16)
GT performance	$\dot{W}_{net(GT)} = \left(\dot{W}_{GT} - \dot{W}_c\right)$	Net output power of GT	(A17)

Table A1. *Cont.*

Module	Equation	Crucial Points	Equation Number
Steam turbine cycle			
Heat recovery steam generator (HRSG) [7]	$\varepsilon = \frac{\dot{m}_{cold} Cp_{cold}(T_{hot} - T_{cold})}{(\dot{m}Cp)_{min}(T_{max} - T_{min})}$	Effectiveness heat exchanger including SHE1 and 2, GTs, HRSG, and ACU	(A18)
	$\varepsilon = \frac{(T_{hot} - T_{cold})}{(T_{max} - T_{min})}$	Effectiveness when $(\dot{m}Cp)_{min} = \dot{m}_{cold} Cp_{cold}$	(A19)
	$\dot{Q}_{lost} = \dot{m}_g \int_{T,cold}^{T,hot} C_{CG} \cdot dT$	Waste energy by exhaust gases	(A20)
	$\dot{Q}_{gained} = \dot{m}_{cold}(h_{hot} - h_{cold})$	Energy earned by water	(A21)
Pumps	$\dot{W}_{ac,p} = \frac{(\dot{m}v(P_{exit} - P_{inlet}))}{\eta_p}$	Work consumed by the pump	(A22)
Mixer	$\sum_{exit} \dot{m}_i h_i = \sum_{inlet} \dot{m}_i h_i$	Conservation of energy to estimate the enthalpy and temperature at the outlet state	(A23)
Steam turbines	$\dot{W}_{s,ST} = \eta_{ST} \dot{m}_{ST}(h_{in} - h_{out})$	Actual steam turbine output power	(A24)
Overall performance	$\dot{W}_{\text{net(ST)}} = \left(\dot{W}_{\text{ac,HPST}} + \dot{W}_{\text{ac,LPST}} - \dot{W}_{\text{ac,p}}\right)$	steam turbine cycle net-work output	(A25)
Solar field system			
Absorber [44]	$\dot{Q}_{u,total} = \dot{m}_{HTF}(h_{si} - h_{soo})$	The parabolic trough collector's useful power rate	(A26)
	$\dot{Q}_u = A_{ap} F_R \left(S - \frac{A_r}{A_{ap}} U_L (T_{soo} - T_a)\right)$	The aperture area is $A_{ap} = (w - D_{c,o})L$	(A27)
	$N_{col} = \frac{\dot{Q}_{u,total}}{\dot{Q}_u}$	Number of collectors is used to calculate $\dot{Q}_{u,total}$, where $N_{col} = Col_r Col_s$, Also, Col_r is collectors in rows and Col_s is collectors in series	(A28)
	$S = G_b \eta_r$	Solar radiation utilized by the PTC tube receiver	(A29)
	$\eta_r = \rho_c \gamma \tau \alpha k_\gamma$	Receiver efficiency, the values for the constants are given in Table 2	(A30)
	$F_R = \frac{\dot{m}_{HTF} Cp_{HTF}}{A_r U_L} \left[1 - \exp\left(\frac{-A_R U_L F_1}{\dot{m}_{HTF} Cp_{HTF}}\right)\right]$	Heat loss coefficient	(A31)
	$F_1 = \frac{U_o}{U_L}$	Efficiency coefficient of the collector	(A32)
	$U_L = \left[\frac{A_r}{(h_{c,ca} + h_{r,ca})A_C} + \frac{1}{h_{r,cr}}\right]^{-1}$	Heat loss between the ambient air and the solar receiver, where receiver surface area $A_r = \pi D_{r,o} L$, and collector surface area $A_c = \pi D_{c,o} L$	(A33)
	$h_{r,cr} = \frac{\sigma(T_c + T_{r,av})\left(T_c^2 + T_{r,av}^2\right)}{\frac{1}{\epsilon_r} + \frac{A_r}{A_C}\left(\frac{1}{\epsilon_{Cv}} - 1\right)}$	Radiative heat transfer coefficient between the tube cover and the receiver where T_c is the receiver temperature, $T_{r,av}$ receiver average temperature and σ is Stefan–Boltzmann constant, whereas ϵ_r and ϵ_{Cv} are given in Table 2.	(A34)

Table A1. *Cont.*

Module	Equation	Crucial Points	Equation Number
Absorber [44]	$h_{r,ca} = \epsilon_{cv}\sigma(T_c + T_a)\left({T_C}^2 + {T_a}^2\right)$	Radiative heat transfer coefficient between the ambient air and the tube cover	(A35)
	$h_{c,ca} = \left(\frac{Nus_a\ K_a}{D_{c,o}}\right)$	Convection heat transfer coefficient between the ambient air and the tube cover, K_a is the thermal conductivity of air	(A36)
	$Nus_a = 0.3Re_a^{0.6}$	Nusselt number for air	(A37)
	$Re_a = \frac{V_a D_{r,o}}{v_a}$	Reynolds number for air assuming the air velocity (V_a) is 5 m/s	(A38)
	$U_O = \left[\frac{1}{U_L} + \frac{D_{r,o}}{h_{c,r,in}D_{r,i}} + \left(\frac{D_{r,o}}{2K_{HTF}} ln\left(\frac{D_{r,o}}{D_{r,i}}\right)\right)\right]^{-1}$	Total heat transfer coefficient between the HTF and surroundings, where K_{HTF} is the HTF conductivity	(A39)
	$h_{c,r,in} = \frac{Nus_{HTF}k_{HTF}}{D_{r,i}}$	Heat transfer coefficient between the receiver and the tube cover	(A40)
	$Nus_{HTF} = 0.023Re_{HTF}^{0.8}Pr_{HTF}^{0.4}$	Nusselt number for the HTF	(A41)
	$Re_{HTF} = \frac{V_{HTF}D_{r,i}}{v_{HTF}}$	Reynolds number for the HTF	(A42)
	$V_{HTF} = \frac{m_{HTF}}{\rho_{HTF}A_{r,cross}}$	Inner velocity for the HTF, where cross area in each tube $A_{r,cross} = 0.25\pi D_{r,i}^2$	(A43)
	$T_c = \frac{h_{r,cr}T_{r,a} + \frac{A_c}{A_r}(h_{c,ca} + h_{\ r,ca})T_0}{h_{r,cr} + \frac{A_c}{A_r}(h_{c,ca} + h_{\ r,ca})}$	Temperature of the receiver cover	(A44)
	$\dot{Q}_{SHE1} = \dot{m}_{HTF}(h_{si} - h_{so})$	Heat input in the SHE1	(A45)
	$h_{2a} = \frac{\dot{Q}_{SHE1}}{\dot{m}_1} + h_2$		(A46)
Inlet air cooling system (Absorption chiller)			
Evaporator	$\dot{Q}_{CL} = \dot{m}_1\ (h_a - h_1)$	Required cooling energy to decrease the temperature of the inlet air by 5 °C	(A47)
	$\dot{Q}_{CL} = \dot{Q}_E$	The heat transferred to the refrigerant	(A48)
	$\dot{Q}_E = \dot{m}_{36}\ (h_{39} - h_{38})$	The energy balance in the evaporator is employed to find the $\dot{m}_{36}$ which is the refrigerant mass flow rate	(A49)
Generator (SHE2)	$\dot{Q}_{Gen,SHE2} = \dot{m}_{42}(h_{42} - h_{43}) + \dot{m}_{36}(h_{36} - h_{42})$	Required heat to run the generator	(A50)
	$\dot{Q}_{Gen,SHE2} = m_{HTF}(h_{so} - h_{soo})$	The state of the HTF at the SHE2 outlet is found using the heat gained in the generator	(A51)
	$\dot{m}_{42} = \frac{x_{42} - x_{36}}{x_{42} - x_{43}} \times \dot{m}_{36}$	$LiBr/H_2O$ mass flow rate with x_i being the concentration at state (i)	(A52)
Absorber	$\dot{Q}_{Abs} = \dot{m}_{39}h_{39} + \dot{m}_{40}h_{40} - \dot{m}_{45}h_{45}$	Heat generated	(A53)
Condenser	$\dot{Q}_{Cond} = \dot{m}_{36}(h_{36} - h_{37})$	Heat produced	(A54)
Solution HE	$\dot{Q}_{Sol,HE} = \dot{m}_{41}(h_{42} - h_{41})$	Heat transfer rate	(A55)

Table A1. *Cont.*

Module	Equation	Crucial Points	Equation Number
Absorption pump	$\dot{W}_{Abs,p} = \dot{m}_{45}(h_{44} - h_{45})$	Power consumed by the absorption pump	(A56)
Thermo-environomic modelling [35]			
Mass flow rate for the NO_x [g/Kg_{fuel}]	$\dot{m}_{NO_x} = \frac{0.15*10^{16}\tau^{0.5}\exp(\frac{-71100}{T_{st}})}{P_3^{0.05}(\frac{\Delta P_3}{P_3})^{0.5}}$	Where T_{st} is the stoichiometric temperature, $\frac{\Delta P_3}{P_3}$ is the normalized pressure drop, τ is the residence time which assumed to be constant (0.002s).	(A57)
Mass flow rate for CO [g/Kg_{fuel}]	$\dot{m}_{CO} = \frac{0.179*10^{9}\exp(\frac{7800}{T_{pz}})}{P_3^{2}\tau(\frac{\Delta P_3}{P_3})^{0.5}}$		(A58)
Adiabatic flame temperature	$T_{pz} = A\sigma^{\alpha}\exp\left(\beta(\sigma+\lambda)^2\right)(\frac{P}{P_{ref}})^{x^*}\theta^{y^*}\psi^{z^*}$	Where θ dimensionless temperature $\frac{T}{T_{ref}}$, ψ is the atomic fuel ratio, x^*, y^*, and z^* are second-degree correlation based on σ, whereas A, α, β are constant, which can be found in [19]	(A59)
Overall system performance analysis			
Overall power	$\dot{W}_{net,} = \dot{W}_{\mathrm{net(GT)}} + \dot{W}_{\mathrm{net(ST)}} - \dot{W}_{Abs,p}$	The total net power	(A60)
Thermal efficiency	$\eta_{CCPP} = \frac{\dot{W}_{net,}}{\dot{m}_{air} LHV\ f}$	The overall efficiency	(A61)
Specific fuel consumption	$SFC = \frac{f\ \dot{m}_{air}}{\dot{W}_{net}}$	-	(A62)

References

1. Furlan, G.; You, F. Robust design of hybrid solar power systems: Sustainable integration of concentrated solar power and photovoltaic technologies. *Adv. Appl. Energy* **2024**, *13*, 100164. [CrossRef]
2. Østergaard, P.A.; Duic, N.; Noorollahi, Y.; Mikulcic, H.; Kalogirou, S. *Sustainable Development Using Renewable Energy Technology*; Elsevier: Amsterdam, The Netherlands, 2020.
3. Akroot, A.; Almaktar, M.; Alasali, F. The Integration of Renewable Energy into a Fossil Fuel Power Generation System in Oil-Producing Countries: A Case Study of an Integrated Solar Combined Cycle at the Sarir Power Plant. *Sustainability* **2024**, *16*, 4820. [CrossRef]
4. Mokheimer, E.M.; Dabwan, Y.N.; Habib, M.A. Optimal integration of solar energy with fossil fuel gas turbine cogeneration plants using three different CSP technologies in Saudi Arabia. *Appl. Energy* **2017**, *185*, 1268–1280. [CrossRef]
5. Liu, X.; Jeffries, J.; Hanson, R.; Hinckley, K.; Woodmansee, M. Development of a tunable diode laser sensor for measurements of gas turbine exhaust temperature. *Appl. Phys. B* **2006**, *82*, 469–478. [CrossRef]
6. Jiang, Y.; Ma, Y.; Han, F.; Ji, Y.; Cai, W.; Wang, Z. Assessment and optimization of a novel waste heat stepped utilization system integrating partial heating sCO_2 cycle and ejector refrigeration cycle using zeotropic mixtures for gas turbine. *Energy* **2023**, *265*, 126326. [CrossRef]
7. Ahmad, A.D.; Abubaker, A.M.; Najjar, Y.S.; Manaserh, Y.M.A. Power boosting of a combined cycle power plant in Jordan: An integration of hybrid inlet cooling & solar systems. *Energy Convers. Manag.* **2020**, *214*, 112894.
8. Dabwan, Y.N.; Zhang, L.; Pei, G. A novel inlet air cooling system to improve the performance of intercooled gas turbine combined cycle power plants in hot regions. *Energy* **2023**, *283*, 129075. [CrossRef]
9. Yao, X.; Yi, B.; Yu, Y.; Fan, Y.; Zhu, L. Economic analysis of grid integration of variable solar and wind power with conventional power system. *Appl. Energy* **2020**, *264*, 114706. [CrossRef]
10. Iraola, A. *U.S. Natural Gas Consumption Set Annual and Monthly Records during 2023*; U.S. Energy Information Administration: Washington, DC, USA, 2024.
11. Rabbani, R.; Zeeshan, M. Exploring the suitability of MERRA-2 reanalysis data for wind energy estimation, analysis of wind characteristics and energy potential assessment for selected sites in Pakistan. *Renew. Energy* **2020**, *154*, 1240–1251. [CrossRef]
12. Kayadelen, H.K.; Ust, Y. Thermoenvironomic evaluation of simple, intercooled, STIG, and ISTIG cycles. *Int. J. Energy Res.* **2018**, *42*, 3780–3802. [CrossRef]
13. Dimitriadis, C.N.; Tsimopoulos, E.G.; Georgiadis, M.C. Optimal bidding strategy of a gas-fired power plant in interdependent low-carbon electricity and natural gas markets. *Energy* **2023**, *277*, 127710. [CrossRef]
14. Al-Otoom, A.; Al-Khalaileh, A.T. Water desalination using solar continuous humidification–dehumidification process using hygroscopic solutions and rotating belt. *Sol. Energy* **2020**, *197*, 38–49. [CrossRef]

15. Hu, H.; Wang, T.; Ren, Y.; Zhang, F.; Zhang, B.; Li, J. A Case Study of Thermal Performance of Gas-Steam Combined Cycle with Gas Turbine Inlet Air Cooling and Condenser Deep Cooling. *Case Stud. Therm. Eng.* **2024**, *60*, 104747. [CrossRef]
16. Archer, C.L.; Jacobson, M.Z. Evaluation of global wind power. *J. Geophys. Res. Atmos.* **2005**, *110*. [CrossRef]
17. Foley, A.M.; Leahy, P.G.; Marvuglia, A.; McKeogh, E.J. Current methods and advances in forecasting of wind power generation. *Renew. Energy* **2012**, *37*, 1–8. [CrossRef]
18. Ondryas, I.; Wilson, D.; Kawamoto, M.; Haub, G. Options in gas turbine power augmentation using inlet air chilling. *J. Eng. Gas Turbines Power U. S.* **1991**, *113*, 203–211. [CrossRef]
19. Barzegar Avval, H.; Ahmadi, P.; Ghaffarizadeh, A.; Saidi, M. Thermo-economic-environmental multiobjective optimization of a gas turbine power plant with preheater using evolutionary algorithm. *Int. J. Energy Res.* **2011**, *35*, 389–403. [CrossRef]
20. Mohapatra, A.K. Thermodynamic assessment of impact of inlet air cooling techniques on gas turbine and combined cycle performance. *Energy* **2014**, *68*, 191–203. [CrossRef]
21. Ehyaei, M.; Hakimzadeh, S.; Enadi, N.; Ahmadi, P. Exergy, economic and environment (3E) analysis of absorption chiller inlet air cooler used in gas turbine power plants. *Int. J. Energy Res.* **2012**, *36*, 486–498. [CrossRef]
22. Nayak, C.K.; Nayak, M.R. Battery Energy Storage System for Solar PV and Wind Power Smoothing Considering Economic Aspects. In *Applications of Computing, Automation and Wireless Systems in Electrical Engineering*; Springer: Berlin/Heidelberg, Germany, 2019; pp. 157–168.
23. Najjar, Y.; Al-Zoghool, Y. Sustainable energy development in power generation by using green inlet-air cooling technologies with gas turbine engines. *J. Eng. Thermophys.* **2015**, *24*, 181–204. [CrossRef]
24. Najjar, Y.S.; Abubaker, A.M.; El-Khalil, A.F. Novel inlet air cooling with gas turbine engines using cascaded waste-heat recovery for green sustainable energy. *Energy* **2015**, *93*, 770–785. [CrossRef]
25. Mahmoudi, S.; Zare, V.; Ranjbar, F.; Farshi, L.G. Inlet Air Cooling Using Absorption Refrigeration. *J. Appl. Sci.* **2009**, *9*, 2399–2407. [CrossRef]
26. Klein, P.; Roos, T.; Sheer, T. Parametric analysis of a high temperature packed bed thermal storage design for a solar gas turbine. *Sol. Energy* **2015**, *118*, 59–73. [CrossRef]
27. Cho, F.; Saito, K. *Fujio Cho Legacy Lecture Notes*; Institute of Research for Technology Development Textbook Gallery: Lexington, KY, USA, 2020; Available online: https://uknowledge.uky.edu/cgi/viewcontent.cgi?article=1000&context=ir4td_textbooks (accessed on 10 September 2021).
28. Mehrpanahi, A.; Naserabad, S.N.; Ahmadi, G. Multi-objective linear regression based optimization of full repowering a single pressure steam power plant. *Energy* **2019**, *179*, 1017–1035. [CrossRef]
29. Colak, H.E.; Memisoglu, T.; Gercek, Y. Optimal site selection for solar photovoltaic (PV) power plants using GIS and AHP: A case study of Malatya Province, Turkey. *Renew. Energy* **2020**, *149*, 565–576. [CrossRef]
30. Najjar, Y.S.; Manaserh, Y.M.A. Aligning combined cycle power plant performance with field measurements. *Arab. J. Sci. Eng.* **2019**, *44*, 1657–1669. [CrossRef]
31. Huld, T.; Müller, R.; Gambardella, A. A new solar radiation database for estimating PV performance in Europe and Africa. *Sol. Energy* **2012**, *86*, 1803–1815. [CrossRef]
32. Heller, P.; Pfänder, M.; Denk, T.; Tellez, F.; Valverde, A.; Fernandez, J.; Ring, A. Test and evaluation of a solar powered gas turbine system. *Sol. Energy* **2006**, *80*, 1225–1230. [CrossRef]
33. Abubaker, A.M.; Ahmad, A.D.; Singh, B.B.; Akafuah, N.K.; Saito, K. Multi-objective linear-regression-based optimization of a hybrid solar-gas turbine combined cycle with absorption inlet-air cooling unit. *Energy Convers. Manag.* **2021**, *240*, 114266. [CrossRef]
34. EU Science Hub. Non-Interactive Service. 2020. Available online: https://joint-research-centre.ec.europa.eu/photovoltaic-geographical-information-system-pvgis/getting-started-pvgis/api-non-interactive-service_en (accessed on 15 September 2021).
35. Yazdi, M.R.M.; Ommi, F.; Ehyaei, M.; Rosen, M.A. Comparison of gas turbine inlet air cooling systems for several climates in Iran using energy, exergy, economic, and environmental (4E) analyses. *Energy Convers. Manag.* **2020**, *216*, 112944. [CrossRef]
36. Singh, H.; Mishra, R. Performance analysis of solar parabolic trough collectors driven combined supercritical CO_2 and organic Rankine cycle. *Eng. Sci. Technol. Int. J.* **2018**, *21*, 451–464.
37. Talbi, M.; Agnew, B. Exergy analysis: An absorption refrigerator using lithium bromide and water as the working fluids. *Appl. Therm. Eng.* **2000**, *20*, 619–630. [CrossRef]
38. Bergman, T.L.; Incropera, F.P.; DeWitt, D.P.; Lavine, A.S. *Fundamentals of Heat and Mass Transfer*; John Wiley & Sons: Hoboken, NJ, USA, 2011.
39. NextEra Energy Partners. Annual Report; 2018. Available online: https://www.investor.nexteraenergypartners.com/~/media/Files/N/NEP-IR/reports-and-fillings/quartely-earnings/2018/q4/4Q18%20NEP%20Earnings%20Release%20FINAL.PDF (accessed on 15 September 2021).
40. Price, H.; Lüpfert, E.; Kearney, D.; Zarza, E.; Cohen, G.; Gee, R.; Mahoney, R. Advances in parabolic trough solar power technology. *J. Sol. Energy Eng.* **2002**, *124*, 109–125. [CrossRef]
41. Al-Sulaiman, F.A. Exergy analysis of parabolic trough solar collectors integrated with combined steam and organic Rankine cycles. *Energy Convers. Manag.* **2014**, *77*, 441–449. [CrossRef]
42. Elsafi, A.M. Exergy and exergoeconomic analysis of sustainable direct steam generation solar power plants. *Energy Convers. Manag.* **2015**, *103*, 338–347. [CrossRef]

43. Kearney, D.; Kelly, B.; Herrmann, U.; Cable, R.; Pacheco, J.; Mahoney, R.; Price, H.; Blake, D.; Nava, P.; Potrovitza, N. Engineering aspects of a molten salt heat transfer fluid in a trough solar field. *Energy* **2004**, *29*, 861–870. [CrossRef]
44. Shahin, M.S.; Orhan, M.F.; Uygul, F. Thermodynamic analysis of parabolic trough and heliostat field solar collectors integrated with a Rankine cycle for cogeneration of electricity and heat. *Sol. Energy* **2016**, *136*, 183–196. [CrossRef]
45. Najjar, Y.S.; Abubaker, A.M. Indirect evaporative combined inlet air cooling with gas turbines for green power technology. *Int. J. Refrig.* **2015**, *59*, 235–250. [CrossRef]
46. Gebreslassie, B.H.; Guillén-Gosálbez, G.; Jiménez, L.; Boer, D. Design of environmentally conscious absorption cooling systems via multi-objective optimization and life cycle assessment. *Appl. Energy* **2009**, *86*, 1712–1722. [CrossRef]
47. National Research Council. *The Ongoing Challenge of Managing Carbon Monoxide Pollution in Fairbanks, Alaska: Interim Report*; National Academies Press: Cambridge, MA, USA, 2002.
48. Saito, K.; Williams, F.; Gordon, A. Structure of laminar coflow methane–air diffusion flames. *ASME J. Heat Mass Transfer* **1986**, *108*, 640–648. [CrossRef]
49. Abubaker, A.M.; Najjar, Y.S.; Ahmad, A.D. A uniquely finned tube heat exchanger design of a condenser for heavy-duty air conditioning systems. *Int. J. Air-Cond. Refrig.* **2020**, *28*, 2050004. [CrossRef]
50. Shi, W.; Pan, L. Optimization study on fluids for the gravity-driven organic power cycle. *Energies* **2019**, *12*, 732. [CrossRef]
51. Najjar, Y.S.; Al-Absi, S. Thermoeconomic optimization for green multi-shaft gas turbine engines. *Energy* **2013**, *56*, 39–45. [CrossRef]
52. Bellos, E.; Tzivanidis, C.; Antonopoulos, K.A. Parametric analysis and optimization of a solar assisted gas turbine. *Energy Convers. Manag.* **2017**, *139*, 151–165. [CrossRef]
53. Wu, C.; Wang, S.-S.; Feng, X.-J.; Li, J. Energy, exergy and exergoeconomic analyses of a combined supercritical CO_2 recompression Brayton/absorption refrigeration cycle. *Energy Convers. Manag.* **2017**, *148*, 360–377. [CrossRef]
54. Edge, E. Overall Heat Transfer Coefficient Table Charts and Equation. 2020. Available online: https://www.engineersedge.com/thermodynamics/overall_heat_transfer-table.htm?fbclid=IwAR2s0hlUqOyWk8_JBl69iV_qVKZM8I6G5Jxi_WulMUA6nDIDwYA14fGhH7k (accessed on 8 September 2020).
55. Abubaker, A.M.; Darwish Ahmad, A.; Salaimeh, A.A.; Akafuah, N.K.; Saito, K. A novel solar combined cycle integration: An exergy-based optimization using artificial neural network. *Renew. Energy* **2022**, *181*, 914–932. [CrossRef]
56. Deymi-Dashtebayaz, M.; Kazemiani-Najafabad, P. Energy, exergy, economic, and environmental analysis for various inlet air cooling methods on Shahid Hashemi-Nezhad gas turbines refinery. *Energy Environ.* **2019**, *30*, 481–498. [CrossRef]
57. Alizadeh, S.; Ghazanfari, A.; Ehyaei, M.; Ahmadi, A.; Jamali, D.; Nedaei, N.; Davarpanah, A. Investigation the Integration of Heliostat Solar Receiver to Gas and Combined Cycles by Energy, Exergy, and Economic Point of Views. *Appl. Sci.* **2020**, *10*, 5307. [CrossRef]
58. Baghernejad, A.; Yaghoubi, M. Exergoeconomic analysis and optimization of an Integrated Solar Combined Cycle System (ISCCS) using genetic algorithm. *Energy Convers. Manag.* **2011**, *52*, 2193–2203. [CrossRef]
59. Amelio, M.; Ferraro, V.; Marinelli, V.; Summaria, A. An evaluation of the performance of an integrated solar combined cycle plant provided with air-linear parabolic collectors. *Energy* **2014**, *69*, 742–748. [CrossRef]
60. Yari, M.; Mahmoudi, S. Utilization of waste heat from GT-MHR for power generation in organic Rankine cycles. *Appl. Therm. Eng.* **2010**, *30*, 366–375. [CrossRef]
61. Ebrahimi, M.; Moradpoor, I. Combined solid oxide fuel cell, micro-gas turbine and organic Rankine cycle for power generation (SOFC–MGT–ORC). *Energy Convers. Manag.* **2016**, *116*, 120–133. [CrossRef]
62. Schwarzbözl, P.; Buck, R.; Sugarmen, C.; Ring, A.; Crespo, M.J.M.; Altwegg, P.; Enrile, J. Solar gas turbine systems: Design, cost and perspectives. *Sol. Energy* **2006**, *80*, 1231–1240. [CrossRef]
63. Alhazmy, M.; Najjar, Y.S. Augmentation of gas turbine performance using air coolers. *Appl. Therm. Eng.* **2004**, *24*, 415–429. [CrossRef]
64. Korakianitis, T.; Wilson, D.G. Models for predicting the performance of Brayton-cycle engines. *J. Eng. Gas Turbines Power* **1994**, *116*, 381–388. [CrossRef]
65. Ameri, M.; Mohammadzadeh, M. Thermodynamic, thermoeconomic and life cycle assessment of a novel integrated solar combined cycle (ISCC) power plant. *Sustain. Energy Technol. Assess.* **2018**, *27*, 192–205. [CrossRef]

Disclaimer/Publisher's Note: The statements, opinions and data contained in all publications are solely those of the individual author(s) and contributor(s) and not of MDPI and/or the editor(s). MDPI and/or the editor(s) disclaim responsibility for any injury to people or property resulting from any ideas, methods, instructions or products referred to in the content.